**Hydrology and Earth System Sciences Discussions**

# Earth observation Water Cycle Multi-Mission Observation Strategy (WACMOS)

Z. Su[1], W. Dorigo[2], D. Fernández-Prieto[3], M. Van Helvoirt[1], K. Hungershoefer[4], R. de Jeu[5], R. Parinussa[5], J. Timmermans[1], R. Roebeling[6], M. Schröder[4], J. Schulz[7,4], C. Van der Tol[1], P. Stammes[6], W. Wagner[2], L. Wang[1], P. Wang[6], and E. Wolters[6]

[1]Faculty of Geo-Information Science and Earth Observation (ITC), University of Twente, Enschede, The Netherlands
[2]Institute of Photogrammetry and Remote Sensing, Vienna University of Technology, Vienna, Austria
[3]European Space Agency, ESRIN, Frascati, Italy
[4]Deutscher Wetterdienst, Satellite Application Facility on Climate Monitoring, Department Climate and Environment, Offenbach, Germany
[5]Department of Hydrology and Geo-Environmental Sciences, Faculty of Earth and Life Sciences, Vrije Universiteit Amsterdam, Amsterdam, The Netherlands

Title Page

| Abstract | Introduction |
| Conclusions | References |
| Tables | Figures |

|◄ | ►|
◄ | ►

Back | Close

Full Screen / Esc

Printer-friendly Version

Interactive Discussion

[6]Royal Netherlands Meteorological Institute (KNMI), De Bilt, The Netherlands
[7]European Organisation for the Exploitation of Meteorological Satellites (EUMETSAT), Darmstadt, Germany

Correspondence to: Z. Su (b_su@itc.nl)

Title Page

Abstract | Introduction

Conclusions | References

Tables | Figures

|◄ | ►|

◄ | ►

Back | Close

Full Screen / Esc

Printer-friendly Version

Interactive Discussion

## Abstract

Observing and monitoring the different components of the global water cycle and their dynamics are essential steps to understand the climate of the Earth, forecast the weather, predict natural disasters like floods and droughts, and improve water re-
5  sources management. Earth observation technology is a unique tool to provide a global understanding of many of the essential variables governing the water cycle and monitor their evolution over time from global to basin scales. In the coming years an increasing number of Earth observation missions will provide an unprecedented capacity to quantify several of these variables on a routine basis. In this context, the European Space
10  Agency (ESA), in collaboration with the Global Energy and Water Cycle Experiment (GEWEX) of the World Climate Research Program (WCRP), launched the Water Cycle Multi-Mission Observation Strategy (WACMOS) project in 2009. The project aims at developing and validating a novel set of geo-information products relevant to the water cycle covering the following thematic areas: evapotranspiration, soil moisture,
15  cloud characterization and water vapour. The generation of these products is based on a number of innovative techniques and methods aiming at exploiting the synergies of different types of Earth observation data available today to the science community. This paper provides an overview of the major findings of the project with the ultimate goal of demonstrating the potential of innovative multi-mission based strategies to im-
20  prove current observations by maximizing the synergistic use of the different types of information provided by the currently available observation systems.

## 1  Introduction

The water cycle is a complex process driven chiefly by solar radiation. The incident radiation evaporates water from water bodies and soil and causes the transpiration from
25  plants. The result of evaporation and transpiration is the presence of water vapour in

Title Page

Abstract | Introduction

Conclusions | References

Tables | Figures

◄ | ►

Back | Close

Full Screen / Esc

Printer-friendly Version

Interactive Discussion

the atmosphere, a prerequisite for cloud formation. If cloud condensation nuclei are present and if the atmospheric state allows for condensation, clouds are formed which are then globally distributed by winds. In the presence of precipitating clouds, water returns back to the Earth's surface where it accumulates in rivers, lakes and oceans.

5 Surface water may also infiltrate into the soil, moistening the soil layers and accumulating as groundwater replenishing aquifers. Aquifers can store water for several years, provide water for human activities, or discharge it naturally to the surface or to the oceans. The response of the hydrological cycle to global warming is expected as far reaching (Bengtsson, 2010), and because different physical processes control the

10 change in water vapour and evaporation/precipitation, a more extreme distribution of precipitation is expected leading to, in general, wet areas wetter and dry areas dryer and as such the changes in the hydrological cycle as a consequence of climate warming may be more severe that the temperature changes.

In this context, relying on accurate and continuous observations of the long-term

15 dynamics of the different key variables governing the above processes from global to local scale is essential to further increase not only our understanding of the different components of the water cycle both in its spatial and temporal variability, but also to characterise the processes and interactions between the terrestrial and atmospheric branches of the energy and water cycle, and how this coupling may influence climate

20 variability and predictability. Such global and continuous observations can only be secured by the effective use of Earth Observation (EO) satellites as a major complement to in-situ observation networks.

In recent years, EO technology has proved to be a major source of data to retrieve an increasing number of hydro-climatic variables, such as radiation, cloud properties,

25 precipitation, evapotranspiration, soil moisture, water vapour, surface water levels, vegetation state, albedo and surface temperature, among others from space (GEO, 2005; ESA, 2006; Schulz et al., 2009; CEOS, 2009; Su, 2010). Such measurements not only have enhanced our capabilities to predict in a reliable manner the variations in the global energy and water cycle but also have provided a key contribution to the

improvement of water governance, the mitigation of water-related natural hazards and the sustainable human development (GEO, 2007; IPCC, 2008).

This paper introduces the Water Cycle Multi-mission Observation Strategy (WAC-MOS) project including its background and objectives (Sect. 2), summaries its products (Sect. 3), its methodologies, retrieval results and validations (Sect. 4) and ends with conclusions (Sect. 5).

## 2   Background and objectives

The past years has seen an increasing earth observation capacity in terms of new missions and sensors. Despite some important improvements in retrieval algorithms and data products, as well as dedicated efforts to better integrate EO-derived products into hydrological models (e.g. Wagner et al., 2009; Su et al., 2010), the full exploitation of EO technology by the hydrological community is still in its early stages. In order to fully exploit this increasing potential and bring this newly available capacity to practical operational levels, significant scientific efforts are required in order to:

  – Develop robust products for which the range of validity and uncertainties are well known and characterised. This will involve the development of robust physically based products supported by a strong validation and inter-comparison exercise;

  – Consolidate the development of consistent long-term data sets integrating different EO systems in a synergetic manner. In this context, the development of long-term consistent data records will rely on equivalent and comparable measurements from different systems and to ensure data consistency separating instrument drifts from geophysical drifts.

  – Develop robust methodologies to integrate and assimilate space observations and in situ measurements into advanced coupled models of biophysical processes

**Earth observation Water Cycle Multi-Mission Observation Strategy**

Z. Su et al.

Title Page

| Abstract | Introduction |
| Conclusions | References |
| Tables | Figures |

|◄ | ►|

◄ | ►

Back | Close

Full Screen / Esc

Printer-friendly Version

Interactive Discussion

and interactions between ocean, land, and atmosphere describing the water cycle and hydrological processes.

In the coming years an increasing number of EO missions will provide unprecedented possibilities to observe the Earth's surface, its interior and the atmosphere, opening a new era in EO and water cycle science and therefore also in hydrology and water resources management. As an example, ESA's Soil Moisture and Ocean Salinity (SMOS) mission (Kerr et al., 2001), launched successfully on 2 November 2009, aims to provide soil moisture information with unprecedented accuracy of $0.04\,\mathrm{m^3/m^3}$ with 3 days of revisiting time and resolutions better than 50 km. Another relevant measurement to the Earth's water budget by SMOS is ocean salinity. These measurements will soon be complemented by NASA's Soil Moisture Active and Passive mission (SMAP) (Enthekabi et al., 2004) planned for launch in 2014-2015 and the Aquarius satellite (http://aquarius.nasa.gov/) for ocean salinity planed for launch in 2011. SMAP will provide global maps of soil moisture and surface freeze/thaw state. Other examples include the Surface Water and Ocean Topography (SWOT) (http://swot.jpl.nasa.gov/), the Global Precipitation Measurement (GPM) mission (http://gpm.gsfc.nasa.gov/), planned to be launched in 2013, and the ESA's EarthCARE mission (ESA, 2004; http://www.esa.int/esaLP/ASESMYNW9SC_LPearthcare_0.html) aiming at improving the representation and understanding of the Earth's radiative balance in climate and numerical weather prediction models. The current requirements for the imager onboard the next third generation of METEOSAT and for the imager onboard Post-EPS foresee water vapour channels within the $\rho\sigma\tau$-water vapour absorption band. MERIS-like observations will be continued on the GMES sentinel 3 mission with the Ocean and Land Colour Instrument (OLCI). Depending on the quality of the final products and final instrument designs an operational processing of several water cycle products seems possible within the next few decades.

In this context, the European Space Agency (ESA) in collaboration with the Global Energy and Water Experiment (GEWEX) of the World Climate Research Program (WCRP) launched the Water Cycle Multi-mission Observation Strategy (WACMOS)

Full Screen / Esc

Printer-friendly Version

Interactive Discussion

project in 2009. The project, funded under the ESA's Support To Science Element, addresses the first two of the above challenges. In particular, the project objective is twofold:

– Developing and validating a novel set of enhanced geo-information products responding to the GEWEX scientific priorities and exploiting the synergetic capabilities between ESA EO data and other non-ESA missions.

– Exploring and assessing different methodologies to exploit in a synergetic manner different observations towards the development of long-term consistent datasets of key hydroclimate variables describing the water cycle.

In this context, WACMOS is focused on four components of the water cycle that are also thematic priorities identified in close collaboration with the GEWEX scientific community: evapotranspiration, soil moisture, clouds and water vapour. The latter three of these components also belong to the Global Climate Observing System (GCOS) Essential Climate Variables (ECVs) for Long-term systematic observation needs of World Climate Research Programme (WCRP) (GCOS, 2006; http://gcos.wmo.int), while the retrieval of the evapotranspiration requires the use of several atmospheric, oceanic and terrestrial ECVs. In this paper, an overview and short summaries are given of each WACMOS component; the more detailed technical descriptions can be found elsewhere in this special issue (Timmermans et al., 2010; Dorigo et al., 2010; Wolters et al., 2010).

## 3 WACMOS products

Table 1 presents a list of WACMOS products, while descriptions of the products, methodology, preliminary results and validations of each product are given in the following separately.

## 3.1 Evapotranspiration

Evapotranspiration (ET) is the process whereby water is transferred from the surface to the atmosphere (Kalma et al., 2008) as a combination of soil and water evaporation and vegetation transpiration. Where the evaporation is only controlled by the physical processes of diffusion and advection, transpiration is also controlled by biological process, like photosynthesis.

Evapotranspiration is unique in providing the link between energy balances, water budgets and plant growth as it plays a vital role in the energy cycle, the water cycle and the carbon cycle (Bowen, 1926; Penman, 1948; Monteith, 1965; Famiglietti and Wood, 1994). By returning available water at the surface to the atmosphere, terrestrial evapotranspiration regulates the biological environment and its water use efficiency. In addition, evapotranspiration is a key parameter for the estimation of plant growth, drought assessment, fire susceptibility and convective precipitation patterns. To be of routine use, all these applications require an evapotranspiration product with the spatial-temporal constraint of 1 km resolution with a 1 day repeat time. Although several methods exist to calculate evapotranspiration from space, still no validated product exists that meets the requirements for routine applications.

The problem with the current algorithms is that they either require local calibration (Bastiaanssen et al., 1998), or they are too complex for global implementation (Kustas and Norman, 2000) and require parameters that cannot be measured correctly from space. The Surface Energy Balance System (SEBS) (Su, 2002) circumvents these problems using physical parameterization (Su et al., 2001) of the turbulent heat fluxes for different states of the land surface and the atmosphere (Obukhov, 1971). For this reason we use SEBS in WACMOS as the baseline algorithm. The algorithm uses three sets of input parameters that can either be measured using remote sensing sensors (like albedo, emissivity, land surface temperature and leaf area index – LAI) or obtained using mesoscale weather models (wind speed, air temperature and humidity,

Title Page

Abstract | Introduction

Conclusions | References

Tables | Figures

|◄ | ►|

◄ | ►

Back | Close

Full Screen / Esc

Printer-friendly Version

Interactive Discussion

and incoming short and long wave radiation). Since evapotranspiration is most sensitive to land surface temperature, a thermal remote sensing sensor is required.

The Advanced Along Track Scanning Radiometer (AATSR) and the Medium resolution Imaging Spectrometer (MERIS) sensor onboard the ENVISAT satellite fit the spatio-temporal requirement of the evapotranspiration product very well; AATSR provides high resolution accurate land and ocean surface temperature measurements and MERIS provides high resolution optical measurements (needed for estimating albedo and LAI). The meteorological parameters have been extracted from the ECMWF database. The meteorological parameters in this database are obtained for both surface height and different pressure levels in the atmosphere, which makes this database highly suitable for scaling between low and high spatial resolutions by employing similarity principles (Su, 2002).

## 3.2 Soil moisture

Recently, GCOS has endorsed soil moisture as one of the Essential Climate Variables (ECV) necessary to characterise the climate of the Earth. It is a variable that has always been required in many disciplinary and cross-cutting scientific and operational applications such as numerical weather prediction, ecology, biogeochemical cycles, flood forecasting, etc. (Jackson et al., 1999). With increasing evidence of climate change, it becomes even more urgent to elucidate the critical role of soil moisture. Since in situ measurements of soil moisture are very sparse, satellite observations in the microwave domain have been broadly recognised as a valuable alternative for capturing its spatio-temporal behaviour.

Soil moisture products from microwave observations dating back to the late 1970s have now become available for several past and present operational radiometers (Njoku et al., 2003; Owe et al., 2008) and scatterometers (Wagner et al., 1999; Bartalis et al., 2007) and will soon be complemented with observations from the recently launched Soil Moisture and Ocean Salinity (SMOS) mission (Fig. 1). Altogether they

Title Page

Abstract | Introduction

Conclusions | References

Tables | Figures

◄ | ►

◄ | ►

Back | Close

Full Screen / Esc

Printer-friendly Version

Interactive Discussion

span a period of more than 30 years facilitating to study long-term soil moisture behaviour e.g. in relation to climate change (Liu et al., 2009).

The scope of the soil moisture theme within WACMOS is to establish a solid scientific basis for the development of long-term consistent soil moisture time series based on active and passive coarse scale microwave observations. The active sensors include the European Remote Sensing satellites (ERS-1 and ERS-2) Scatterormeter (SCAT), the Meteorological Operational satellite (MetOp) Advanced Scatterometer (ASCAT) and the passive sensors include the Scanning Multichannel Microwave Radiometer (SMMR), the Special Sensor Microwave Imager (SSM/I), the Tropical Rainfall Measuring Mission (TRMM), the Advanced Microwave Scanning Radiometer – Earth Observing System (AMSR-E) and the Windsat, Despite the large increase in temporal coverage that potentially can be obtained by combining the data sets, the use of multi-mission data involves many scientific challenges as well, since the climatologies of the different products need to be harmonised and the complex effects of the various error sources (sensor calibration, retrieval errors, model parameterisation, etc.) on observed variations need to be understood for each product and sensor. In this study we propose a first concept for such a merging scheme, based on the ERS and ASCAT scatterometers and the AMSR-E, TRMM, and SSM/I radiometers.

## 3.3 Cloud products

Clouds and precipitation play an essential role in the energy budget and hydrological cycle of the Earth. Clouds reflect shortwave radiation and trap longwave radiation, and thus modulate surface incoming fluxes at short- and long wavelengths. Moreover, clouds are the visible expression of atmospheric condensation processes, and are the prerequisite for precipitation, which is essential for many processes on land. Quantitative estimates of cloud and precipitation properties at high spatial and temporal resolutions are of increasing importance for water resource management, and for improving our understanding of precipitation processes in climate and weather forecasting models. Although operational networks of weather radars are expanding over

**Earth observation Water Cycle Multi-Mission Observation Strategy**

Z. Su et al.

Title Page

| Abstract | Introduction |
| Conclusions | References |
| Tables | Figures |

Back | Close

Full Screen / Esc

Printer-friendly Version

Interactive Discussion

Europe and North America, large areas remain where information on precipitation is lacking. Precipitation estimates from passive imagers may bridge this gap. Polar orbiting satellites can provide information on seasonal and inter-annual variations of cloud and precipitation properties at the global scale while geostationary satellites can provide information on diurnal variations at quasi-global scales. The properties of importance to the WACMOS project are Solar Surface Irradiance (SSI), Cloud Water Path (CWP) and precipitation occurrence and intensity (PRP).

The SSI is basically the transmission of solar incoming radiation at the top-of-atmosphere (TOA) to the surface, which is mainly determined by the cloud fraction, the cloud optical thickness, and the amount of water vapour and aerosols in the atmosphere. It is of importance to the Evapotranspiration theme, since the amount of SSI determines the amount of energy available for the evaporation from the surface and transpiration from the canopies. The precipitation *occurrence* is determined from Cloud Water Path (CWP), effective radius, and cloud phase information, whereas the precipitation *intensity* is calculated from CWP and the thickness of the raining column, which in turn is estimated from the difference between the temperature of the surface and the cloud-top. Observations from the Spinning Enhanced Visible and InfraRed Imager (SEVIRI) onboard Meteosat Second Generation (MSG) combined with water vapour profiles from the MEdium Resolution Imaging Spectrometer (MERIS) on board ENVISAT are used to obtain these cloud properties at regional scale and at high temporal resolution i.e., Level 2 products that are generated every hour or even every 15 min in case of SEVIRI. The latter temporal resolution is required for regional water and energy balance studies. Observations from the SCanning Imaging Absorption spectroMeter for Atmospheric CartograpHY (SCIAMACHY) onboard the polar orbiting satellite ENVISAT are used to derive SSI and CWP at global scale. Time series of SCIAMACHY observations, complemented with observations from its predecessor GOME and GOME-2, provide a solid basis for the generation of Thematic Climate Data Records of SSI and CWP, and thus contribute to the comprehensive system of Atmospheric ECVs endorsed by GCOS (GCOS, 2010).

## 3.4 Water vapour

Water vapour is a key variable in the Earth's water and energy cycle. In the lower troposphere, water vapour is the main resource for clouds and precipitation and the related latent heating dominates the structure of tropospheric diabatic heating (Trenberth and Stepaniak, 2003). In addition, water vapour varies strongly in space and time, is the most effective greenhouse gas, and climate models indicate a strong positive radiative feedback (Held and Soden, 2000). Satellite observations provide near-global coverage and thus represent an important source of information, especially over the oceans, where radiosonde observations are scarce, and in the upper troposphere, where radiosonde sensors are often unreliable. There are about 50 satellite missions that are capable to retrieve atmospheric profiles of humidity or the total column amount (Hollweg, 2005). Various spectral ranges (microwave, infrared, visible, ultraviolet), observation geometries (nadir, limb, occultation) and retrieval techniques are utilised, each having their own advantages and disadvantages. WACMOS aims at exploring novel methodologies to deliver enhanced water vapour products that exploit the synergies among different observation systems. Two combined products of water vapour from three different sensors, namely the METEOSAT Second Generation (MSG) Spinning Enhanced Visible and Infrared Imager (SEVIRI), the Environmental Satellite (ENVISAT) Medium Resolution Imaging Spectrometer (MERIS) and the Meteorological Operational satellite (MetOp) Infrared Atmospheric Sounding Interferometer (IASI), are developed. The first product combines the high vertical sampling and expected high quality of METOP/IASI measurements with the high temporal sampling of MSG/SEVIRI data to provide a combined product covering the complete African continent and Central Europe. The second product is based on MSG/SEVIRI measurements and ENVISAT/MERIS data featuring a high spatial resolution. This product will be provided over land only because the MERIS instrument is not capable to observe total column water vapour over oceans with high accuracy and precision. Both WACMOS water vapour products will be generated under clear sky conditions only,

Title Page

| Abstract | Introduction |
| Conclusions | References |
| Tables | Figures |

◀◀  ▶▶

◀  ▶

Back  Close

Full Screen / Esc

Printer-friendly Version

Interactive Discussion

because at infrared and near-infrared wavelengths clouds are opaque and do not allow water vapour retrieval. Based on the requirements for water vapour profiles for global numerical weather prediction and climate modelling given by World Meteorological Organization (WMO) (WMO/ReqObs, 2001; WMO/GCOS, 2006) and taking into account the instrument designs, the following technical specification was defined for the proposed WACMOS water vapour products: The combined SEVIRI + IASI water vapour product will provide tropospheric water vapour for at least three layers (200-500 hPa, 500–850 hPa, 850 hPa – surface) at the full MSG disc with a horizontal resolution of 0.25° and will be generated for the period from June 2008 to May 2009. The SEVIRI + MERIS product will provide the total column water vapour for northeast Europe on a 0.025° grid for the time period between June and November 2008. A three-hourly temporal resolution (00:00-03:00 UTC, 03:00–06:00 UTC, etc.) is foreseen for both products. In order to be valuable for use in global numerical weather prediction and climate monitoring, uncertainty requirements are defined for both products. The accuracy (precision) for the combined SEVIRI + IASI product is expected to be better than 0.2 (0.8), 0.6 (2.0) and 0.8 (3.0) $\mathrm{kg\,m^{-2}}$ for the top, middle and bottom layer, respectively. Total column water vapour accuracy and precision for the SEVIRI + MERIS product are expected to be at least 1 $\mathrm{kg\,m^{-2}}$ and 4 $\mathrm{kg\,m^{-2}}$.

## 4  Methodology, retrieval results and validations

### 4.1  Evapotranspiration: methodology, results and validation

#### 4.1.1  Evapotranspiration: methodology

Evapotranspiration cannot directly be measured from space. Therefore most current algorithms calculate the evapotranspiration through the energy balance equation (Kustas and Norman, 2000; Anderson et al., 2008; van der Tol et al., 2009a). In this energy balance equation the net radiation, ground heat flux, and sensible heat flux can be

estimated from remote sensing imagery. During the last 50 years, a wide range of methods have been developed and evaluated (Glenn et al., 2007; Kalma et al., 2008). The difference between the different methods is the way in which the sensible heat term in the energy balance equation is calculated.

The Surface Energy Balance System (SEBS) model (Su, 2002) is the only single source algorithm that calculates the sensible heat through physical representation of the turbulent heat exchange. The SEBS algorithm incorporates explicitly the formulation of the roughness height for heat transfer, instead of using fixed values (Su et al., 2001). Since the roughness height for heat transfer can vary with geometrical and environmental variables in several orders of magnitude for different surface types, ignoring the spatial variability of roughness height has led to great uncertainties in estimation of heat fluxes or evaporation using radiometric temperature measurements in several algorithms (e.g. Kalma et al., 2008). Although it is possible to calibrate these algorithms such that their estimates reproduce observations at local scale (e.g. Bastiaanssen et al., 1998), it would be very difficult to extend them to regional/continental studies by means of satellite observations. These shortcomings are avoided in SEBS.

The turbulent character of the sensible heat is represented by the use of the similarity theories (Kolmogorov, 1991). SEBS iterates over a set of similarity equations using Monin-Obukhov Similarity Theory (Monin and Obukhov, 1954) and Bulk Atmospheric Similarity Theory (Brutsaert, 1999) that characterize the turbulent exchange of momentum, heat and water vapour. In SEBS, the sensible heat is further constrained by relative evaporative fraction, which is determined by comparing this sensible heat flux to sensible heat for theoretical wet and dry conditions in order to characterize crop stress. SEBS is therefore capable of estimating evapotranspiration without the need for local calibration or large numbers of input parameters. It uses three sets of input parameters for the determination of ET instead. The first set consists of remotely sensed vegetation parameters, like surface albedo, emissivity and surface temperature. The second set includes meteorological observations, like air temperature, vapour pressure and air pressure. The third set of data includes remotely sensed parameters like

incoming long and shortwave radiation. In WACMOS these parameters sets are obtained through AATSR/MERIS, MODIS, MSG sensors and ECMWF model outputs (see Tables 2 and 3). An example of the surface fluxes from MODIS over the Netherlands on 6 January 2008 is shown in Fig. 2. Instantaneous values for the surface heat fluxes are scaled up to daily values using the evaporative fraction.

### 4.1.2 Evapotranspiration: results and validation

Actual latent heat flux cannot be measured directly from remote sensing imagery, but needs to be estimated as the "residual" of the energy balance equation. Thus, besides the validation using ground based measurements, the estimation of the actual evapotranspiration can be validated by validating the individual components of the energy balance equation: net radiation, sensible heat flux and ground heat flux. In addition, the upscaling technique from instantaneous to daily evapotranspiration needs an evaluation too. These validations are currently hardly possible, because no global products of net radiation, ground heat flux, or sensible heat flux exist for comparison. At last, the validation needs to be performed against field measurements.

The ground based measurements that are mostly used are the Bowen ratio method (Pauwels and Samson, 2006), eddy covariance (Baldocchi et al., 2001) and scintillometry (Kite and Droogers, 2000; Pauwels et al., 2008). In the Bowen ratio method the energy balance is partitioned into a part that is used for sensible heat and a part that is used for latent heat. The ratio of these two is the Bowen ratio, which is controlled by the difference in air temperature and humidity at two heights in the air above the canopy. In the eddy covariance method the latent heat flux is estimated directly by measuring the water vapour concentration in upward and downward eddies, simultaneously with their velocity. In scintillometry the sensible heat flux is calculated by measuring the refraction index of the air over a specified distance.

The validation is troubled because of scale differences between field measurements and the remote sensing imagery. Not only do the field measurements have a different

footprint (only the scintillometer measurement has a footprint in the order of the pixel size of the WACMOS product), the revisit time of certain satellites also prohibits comparison of long time series. The revisit time of the remote sensing sensors combined with cloud cover limit the number of remote sensing images that can be used for vali-

5  dation purposes. This problem is circumvented by using the Soil Canopy Observation, Photochemistry and Energy fluxes (SCOPE) model (van der Tol et al., 2009b) to interpolate between satellite overpasses. SCOPE is also used as a remote sensing product simulator.

The SCOPE model is a soil-vegetation- atmosphere model that couples radiative
10  transfer of optical and thermal radiation with leaf biochemistry processes. It is able to simultaneously estimate from the meteorological forcing the vertical distribution of within-canopy canopy heat flux, the aerodynamic resistances (Verhoef et al., 1999) and the hyperspectral outgoing radiances (Verhoef et al., 2007). These radiances can be used as input for a sensor simulator that is attached to the model. The advantage
15  of simulating AATSR radiances is that uncertainties in the atmospheric correction are circumvented and that we have "measurements" even for clouded days. The model therefore provides both the parameters needed as input for SEBS (meteorological parameters, the remote sensing imagery) and the parameters that need to be validated (surface fluxes) such that the parameterizations in SEBS can be evaluated.

20  In the validation presented here new parameterizations for the estimating LAI, ground heat flux and the roughness length for heat transfer are discussed (Timmermans et al., 2010). The data used for validation of the new ground heat flux formulation was measured at Sonning site by the University of Reading. The methodology is to evaluate/validate the individual heat fluxes (Figs. 3 and 4) and afterwards evaluate the
25  methodology for interpolating actual evapotranspiration to daily values (Fig. 5). The original parameterizations caused an underestimation of the soil heat flux and sensible heat flux. The underestimation of the soil heat flux originated due to the use of the fractional vegetation cover. This parameter tends to saturate very quickly to values for full canopy, although ground measurements showed otherwise. The new parameterization

Title Page

Abstract | Introduction

Conclusions | References

Tables | Figures

◄◄ | ►►

◄ | ►

Back | Close

Full Screen / Esc

Printer-friendly Version

Interactive Discussion

solved this problem by incorporating the leaf area index for separation between bare soil and fully developed vegetation instead.

In SEBS the actual evapotranspiration is extrapolated to daily values using the evaporative fraction which is considered constant during the day. However, Fig. 5 shows that in wintertime the evaporative fraction has not reached its equilibrium state at the time of the satellite overpass. This can cause an overestimation of the daily evapotranspiration during this season. The solution for this problem is to use geostationary satellite imagery to estimate the diurnal pattern of evaporative fraction and correct for this effect.

## 4.2 Soil moisture: methodology, results and validation

### 4.2.1 Soil moisture: methodology

The proposed soil moisture merging scheme can be subdivided into three components: error characterisation, rescaling, and merging. Characterising the uncertainty of the individual data sets is required to decide for each location which data set provides the most reliable soil moisture estimates and, therefore, should be favoured in the merged product. Rescaling of the different data sets is needed to bring the different data sets into a common observation space. The merging itself combines the different data sets into a single product. It was decided to merge the data sets in two successive stages: First, all radiometer-based soil moisture observations are merged to a single passive soil moisture time series and all scatterometer-based soil moisture observations are merged to a single active soil moisture time series; Second, the resulting active and passive time series are combined into a final multi-sensor product.

**Step 1: error characterisation by triple collocation**

The triple collocation method allows a simultaneous estimation of the random error structure and the cross-calibration of a set of at least three linearly related datasets

with uncorrelated errors (Scipal et al., 2008; Dorigo et al., 2010). We can fulfil this requirement if we combine one of the scatterometer-, and one of the radiometer-based soil moisture data sets with a globally available modelled soil moisture data set. The GLDAS-NOAH reanalysis data set is a suited candidate for this purpose. Implemen-
tation of the triple collocation method was done following Miralles et al. (2010), who considered soil moisture anomalies from the long-term mean instead of the original soil moisture values. As true soil moisture values are unknown, one of the input data sets must be chosen as a reference against which both other data sets are rescaled. We chose GLDAS-NOAH as the reference data set which means that all resulting er-
rors are expressed in the climatology of this data set. Theoretically, an infinite number of common observations are required to obtain unbiased estimates with the triple collo-cation technique but a minimum number of 100 triples appear to be a good practicable trade-off (Scipal et al., 2008). Hence, areas with less than 100 triplets are masked in the results. The triple collocation was repeated for different combinations of active,
passive and GLDAS-NOAH data in order to obtain error estimates for all satellite based soil moisture products.

**Step 2: rescaling**

Systematic differences between the different data sets result either from differences in observation principle and retrieval method (active versus passive), from differences in
frequency (for the passive systems), and different sensor specifications (applies both to active and passive data sets). Cumulative distribution function (CDF)-matching is used to bridge these systematic differences (Drusch et al., 2005; Liu et al., 2009).

First, all radiometer soil moisture observations are rescaled into the climatology of AMSR-E, as this sensor is known to provide the most reliable soil moisture estimates
and climatology of all considered passive systems. Similarly, for the active systems the ERS observations are rescaled into the climatology of ASCAT.

As neither the active nor one of the passive systems can provide a complete global and temporal coverage of soil moisture estimates, none of these data sets can be used

Title Page

Abstract | Introduction

Conclusions | References

Tables | Figures

◄ | ►

◄ | ►

Back | Close

Full Screen / Esc

Printer-friendly Version

Interactive Discussion

as a reference to which the other data set is rescaled. Therefore, we used the GLDAS-NOAH soil moisture data set as a reference against which the active and passive merged products are adjusted. As a result, all soil moisture data sets are expressed in the same climatology. CDF-matching was applied for each grid point individually.

5 **Step 3: data set merging**

First, all rescaled passive and active soil moisture data sets are merged to a single radiometer- and scatterometer-based soil moisture time series, respectively. For each time step, this is done by averaging the available data sets. If an observation is available for only one data set, its value is directly incurred in the merged product.

10 Based on the error maps resulting from the triple collocation, areas can be identified where either (i) scatterometers perform better than radiometers, (ii) radiometers outperform the scatterometers, or (iii) both data sets perform equally well. In the areas where one of the first two conditions applies, only the active or passive data set is used respectively, because introducing the less performing data set would deteriorate

15 the final product. In areas where both data sets perform equally well, it is first tested whether both data sets are highly correlated, which is a clear indication that both data sets describe the same phenomenon. Only highly correlated data sets ($r > 0.6$) are merged, otherwise only the passive observations are used. If the condition of high correlation is met, the active and passive data sets are combined in the following way: On

20 time steps where observations from both data sets are available, these are combined by simple averaging. On time steps where either one of the data sets is available, it is directly ingested into the final product. More details on the merging process can be found in (Liu et al., 2010).

### 4.2.2 Soil moisture: results and validation

25 Concerning the results of the triple collocation, Fig. 6 shows the triple collocation errors for a combination of ASCAT, AMSR-E C-band, and GLDAS-NOAH soil moisture

estimates. The errors are expressed in the climatology of the GLDAS-NOAH re-analysis data set which was used as a reference. Generally, error estimates are lowest in arid regions such as Southern Africa, mainland Australia or Central Asia which is explained by the very low amounts of precipitation received and hence the very low

5  variability of soil moisture.

Several characteristic differences in the spatial distribution of the errors can be observed between the data sets. In very dry areas errors of soil moisture derived from AMSR-E C-band are remarkably lower than soil moisture estimates derived from AS-CAT. This is a phenomenon caused by a combination of volume scattering effects in

10  dry, loose sand and increased sensitivity of backscatter to linear micro-topographic features like sand dunes. On the other hand, soil moisture derived from AMSR-E is prone to larger random errors in moderately to densely vegetated areas. With increasing vegetation density, radiance emitted from the soil surface is increasingly absorbed by the vegetation canopy and the observed emissivity will be due largely to the vegeta-

15  tion. The results observed for ASCAT and AMSR-E are generally representative for all active and passive soil moisture sensors considered in this study, although for higher radiometer frequencies the errors increase in moderately to densely vegetated areas due to increased attenuation by the canopy of radiation emitted from the soil surface.

Figure 7 shows the areas where radiometer-based (blue) or scatterometer-based

20  (red) soil moisture is outperforming the other. In these areas only the respective product is propagated to the merged product. The orange colours in the figure indicate areas where triple collocation errors of active and passive data sets are very similar and where both data sets are highly correlated ($R > 0.6$). These areas coincide with transition zones between humid and dry areas and typically show high seasonal soil

25  moisture and vegetation dynamics. In these areas the merged soil moisture product will be based on both active and passive data.

Concerning the results of the data merging process, for the period of common AS-CAT and AMSR-E observations (i.e. the years 2007 and 2008), the merged product contains significantly more observations (here expressed as the percentage of the total

Title Page

Abstract | Introduction

Conclusions | References

Tables | Figures

◄◄ | ►►

◄ | ►

Back | Close

Full Screen / Esc

Printer-friendly Version

Interactive Discussion

observation for which an observation is available) than each of the single data products (Liu et al., 2010). Especially in these regions, an increased number of observations are of high importance as here soil moisture contents are highly variable and higher temporal frequency observations may lead to a better understanding of atmosphere-land interactions.

Figure 8 exemplifies for a transition region in Australia the effect of merging AMSR-E and ASCAT retrievals. The original data sets are not only highly correlated with each other but also with the local in-situ measurements taken at the OzNet site (Young et al., 2008). It is shown that the merged product has a correlation with the in-situ measurements which is comparable to those of the input products and that the number of days for which observations are available are considerably increased. Nevertheless, compared to the original AMSR-E data also a bias is introduced due to rescaling the observations into the climatology of GLDAS-NOAH.

As a preliminary analysis of the final results, Fig. 9 shows the global distribution of average soil moisture content calculated from the merged data set. Calculating the climatology from the merged data set instead of from the single sensor products provides more reliable estimates in both very dry and vegetated areas, and hence a more complete global picture. It should however be recalled that the merged data set is expressed in the dynamic range of GLDAS-NOAH so even though the relative patterns are plausible, the absolute values should be taken with caution.

The multi-sensor data set gives us the opportunity to compute the average changes in soil moisture over the period of observation (i.e. 1992–2008; Fig. 10). We see some areas where clear increases (e.g. Southern Africa) or decreases (e.g. Kazakhstan) occurred over the last two decades. Independent data sets and observations seem to confirm the observed trends. For example the long term increase of soil moisture in southern Africa is confirmed by positive trends in the Zambezi and Okavango river (Mazvimavi and Wolski, 2006). However, these trend maps need to be studied in more detail before final conclusions can be drawn.

## 4.3 Clouds products: methodology, results and validation

### 4.3.1 Cloud products: methodology

The retrieval of Solar Surface Irradiance (SSI), precipitation occurrence and precipitation intensity from SEVIRI is physically based, and relies on information of the cloud optical properties (cloud optical thickness) and physical properties (cloud condensed water path, cloud phase, and cloud particle effective radius) derived with the Cloud Physical Properties (CPP) algorithm (Roebeling et al., 2006) of the SAF on Climate Monitoring (CM-SAF) (Schulz et al., 2009), and water vapour profiles from the MEdium Resolution Imaging Spectrometer (MERIS) on board ENVISAT. The CPP algorithm retrieves cloud optical thickness, cloud particle effective radius, and cloud thermodynamic phase from observed cloud reflectances at visible (0.6 µm) and near infrared (1.6 µm) wavelengths following the method described by Nakajima and King (1990). The cloud top temperature and height are retrieved from visible (0.6 µm) reflectances and infrared (10.8 µm) cloud radiances (Minnis, 1998). The condensed water path is computed from the retrieved cloud optical thickness and cloud particle effective radius. The retrieval of cloud optical thickness, particle size and cloud phase is done iteratively by matching satellite observed reflectances to look-up tables (LUTs) of simulated reflectances of horizontally and vertically homogeneous water and ice clouds, generated with the Doubling Adding KNMI (DAK) radiative transfer model (Stammes, 2001). The phase "ice" is assigned to pixels for which the observed visible and near-infrared reflectances correspond to simulated reflectances of ice clouds and the cloud top temperature is lower than 265 K. The remaining cloudy pixels are considered to represent water clouds. Note that the cloud properties retrievals rely on visible and near-infrared observation, and thus are limited to satellite and solar viewing zenith angles smaller than 72°.

The retrieval of SSI from SEVIRI and MERIS observations is based on the algorithm described by Deneke et al. (2008). This algorithm takes into account variability induced

by cloud optical thickness, cloud phase, and particle size from SEVIRI, surface albedo from MODIS, and total precipitable water from MERIS, while for other sources of variability climatological means are used. In its current version, the changes in aerosol properties are neglected. Obviously, this is the largest source of error, in particular for clear sky conditions, while neglecting these properties for cloudy conditions has minor consequences. Radiative transfer simulations are done off-line with the discrete ordinate method for radiative transfer in vertically inhomogeneous layered media (DISORT) (Stamnes et al., 1988). An example of the SSI product is presented in Fig. 11.

The retrieval of global SSI from SCIAMACHY is based on the MAGIC algorithm of Mueller et al. (2009) and the FRESCO+ (Fast Retrieval Scheme for Clouds from the Oxygen A-band) algorithm of Wang et al. (2008). The MAGIC algorithm has a look-up-table for the retrieval of clear-sky SSI, taking into account the variability in aerosol properties, water vapour column, surface albedo, and solar zenith angles. For the cloudy pixels (including fully or partly cloudy pixels) MAGIC needs information on the cloud index, which is retrieved from SCIAMACHY observations with the FRESCO+ algorithm. Although SCIAMACHY observes at a low spatial resolution ($30 \times 60\,\mathrm{km}^2$), its high spectral resolution at ultraviolet, visible, and near infrared wavelengths enables a novel type of observation of clouds. The FRESCO+ algorithm retrieves the effective cloud fraction, which is directly related to the cloud index of the MAGIC algorithm, and cloud pressure from the TOA re?ectance at three wavelengths (758, 760, and 765 nm). Due to the presence of clouds, the reflectance at 758 nm is larger than for a clear-sky scene, whereas the depth of the strongest $O_2$ absorption band at 760 nm and of the weaker $O_2$ absorption band at 765 nm varies according to the height and the optical thickness of the cloud. The FRESCO+ algorithm fits a simulated reflectance spectrum to the measured reflectance spectrum for the three wavelengths to retrieve the effective cloud fraction and cloud pressure. The SCIAMACHY SSI product is generated from the FRESCO orbit data (Level 2) and is regridded to monthly mean global maps. Figure 12 shows an example of the global monthly mean SSI for July 2008 as retrieved from SCIAMACHY. The latitudinal gradient of surface solar irradiance is clearly observed

from the monthly mean map. The ITCZ and stratocumulus cloud fields at the west of the continent show low SSI and high SSI occurs in the Sahara desert.

The retrieval of precipitation occurrence and intensity is based on the approach presented by Roebeling and Holleman (2009). Their approach uses information on condensed water path, particle effective radius, and cloud thermodynamic phase to detect precipitating clouds, while information on condensed water path and cloud top height is used to estimate rain rates. A simple but adequate model proposed by Petty (2001) is used to calculate evaporation of rainfall below cloud base. This procedure uses water vapour retrievals from monthly mean MERIS, and cloud top height and optical thickness retrievals from SEVIRI to estimate the height of the cloud base. The fact that their approach can be applied to geostationary observations from SEVIRI potentially allows for the provision of precipitation observations over the full MSG disk, covering Europe and Africa every 15 min. Examples of the monthly mean precipitation occurrence and intensity products are presented in Fig. 13.

## 4.3.2 Cloud products: results and validation

The Solar Surface Irradiance products from SCIAMACHY and SEVIRI are validated against ground-based measurements of the Baseline Surface Radiation Network (BSRN). Figure 14 shows for the BSRN station of Cabauw (the Netherlands) that instantaneous SSI retrievals from SCIAMACHY and SEVIRI agree well with hourly averaged irradiance values during May 2006. During this month the precision (RMS) is about $75\,\mathrm{W\,m^{-2}}$ for SCIAMACHY and about $35\,\mathrm{W\,m^{-2}}$ for SEVIRI, while both instruments have an accuracy (bias) better than about $8\,\mathrm{W\,m^{-2}}$. The results for Cabauw are in line with the findings of Deneke et al. (2008), who validated an earlier version of the SSI algorithm with one year of pyranometer measurements from 35 stations over the Netherlands. Because the Cabauw station is located in a flat and homogenous grassland terrain at sea level, the BSRN measurements taken at this station are more likely to represent the area of a satellite pixel. At BSRN stations that are located in more heterogeneous terrain larger variations between satellite retrieved and BSRN

Title Page

Abstract | Introduction

Conclusions | References

Tables | Figures

◄ | ►

◄ | ►

Back | Close

Full Screen / Esc

Printer-friendly Version

Interactive Discussion

observed SSI values are expected. For example, due to the height above sea level, horizontal view restrictions, multiple reflection effects, or shadow effects. Especially the SCIAMACHY retrievals, which represent an area of $30 \times 60\,km^2$ at nadir, are subject to lower precision over heterogeneous terrains. The SSI retrievals from SEVIRI, which have a spatial resolution of $3 \times 3\,km^2$ at nadir, will be more precise over heterogeneous terrain. The latter precision may further improve when KNMI introduces an improved SSI product for SEVIRI that also uses information from the high-resolution visible (HRV) channel (Deneke and Roebeling, 2010).

The precipitation occurrence and intensity products from SEVIRI are validated against two types of reference instruments i.e., the Tropical Monsoon Measurement Mission Precipitation Radar (TRMM-PR) and ground-based weather radar observations. The validity of these products was demonstrated over central Europe by Roebeling and Holleman (2009) and over western Africa by Wolters et al. (2010). Although both papers validate the SEVIRI precipitation products over different climate regions and with different reference instruments, similar validation results are found. Over central Europe (50° N–55° N, 3° E–8° E) the SEVIRI precipitation products were compared to corresponding weather radar observations for a period of two months. Over western Africa (20° S–20° N, 20° W–20° E) the SEVIRI precipitation products were compared to 127 TRMM-PR overpasses. Figure 15 presents the relationship between SEVIRI retrieved and reference instrument observed areal mean precipitation occurrence and rain rate. It can be seen that the areal mean precipitation occurrences from SEVIRI and the reference instruments are highly correlated (corr. $\approx 0.9$), while the areal mean rain rate retrievals are weaker correlated (corr. $\approx 0.6$). At pixel level, the SEVIRI retrievals have an acceptable accuracy (bias) of about $0.1\,mm\,h^{-1}$ and a precision (standard error) of about $0.8\,mm\,h^{-1}$ (Roebeling and Holleman, 2009). Mismatches between the re-projected SEVIRI and reference instrument images, due to differences in observation time, parallax shifts and collocation errors, hinder the comparison of both images. Here, the parallax shift is the apparent displacement of an observed cloud, which occurs because SEVIRI observes the Earth under an oblique angle.

## 4.4 Water vapour: methodology, results and validation

### 4.4.1 Water vapour: methodology

Input parameters to the products are SEVIRI Level 1.5 data that are navigated and calibrated brightness temperatures, MERIS reduced resolution total column water vapour with a spatial resolution of 1.2 km and the water vapour profiles (90 vertical levels) obtained from IASI. The retrieval of the MERIS water vapour content has been performed using the algorithms described in Fischer and Bennartz (1997) as well as Bennartz and Fischer (2001). The EUMETSAT (European Organisation for the Exploitation of Meteorological Satellites) operational IASI level 2 product processing is described in Schlüssel et al. (2005). MERIS and IASI data are operationally processed and provided by ESA and EUMETSAT, respectively. SEVIRI water vapour estimates are obtained employing a physical retrieval scheme (NWC SAF PGE 13 ATBD, 2009) developed within the EUMETSAT Satellite Application Facility (SAF) on Support to Nowcasting and Very Short-Range Forecasting (NWC SAF). Although SEVIRI infrared brightness temperatures contain information on approximately three broad atmospheric layers, retrieved SEVIRI water vapour profiles have 43 vertical levels. This is done because the simulation of the SEVIRI instrument within the physical retrieval approach requires a certain vertical resolution. Since the retrieval is done for clear sky pixels only, the SEVIRI cloud mask, part of the NWC SAF MSG software package and available from the Climate SAF (CM SAF), is a mandatory retrieval input. The cloud mask algorithm used is described in Derrien and LeGléau (2005). The SEVIRI total column water vapour (TCWV) is determined by vertically integrating the water vapour profiles. Since the IASI and SEVIRI retrieval are based on optimal estimation theory, a measure of uncertainty is obtained as well. In case of MERIS, an uncertainty of 10% relative to the water vapour amount is assumed for land pixels (MERIS PQSR, 2006).

For both WACMOS water vapour products an objective analysis method (Kriging) is applied to interpolate data in space and time with the possibility to also provide uncertainty information for the combined products. Kriging is a geostatistical method which

Title Page

Abstract | Introduction

Conclusions | References

Tables | Figures

◄ | ►|

◄ | ►

Back | Close

Full Screen / Esc

Printer-friendly Version

Interactive Discussion

is currently applied in diverse disciplines like e.g. hydrology (Goovaerts, 2000) and me-
teorology (Lindenbergh et al., 2008). The approach of Lindenbergh et al. (2008), who
combined MERIS TCWV observations with hourly ground based Global Positioning
System (GPS) observations of a single day, is applied. In case of the SEVIRI + MERIS
product, the combined integrated total water vapour column $\hat{x}(p_0, t_s)$ at location $p_0$
and time $t_S$ (i.e. one grid point and 3-h interval) is predicted as a linear combination

$$\hat{x}(p_0, t_S) = \sum_{i=1}^{n} \lambda_i (x_S(p_i, t_S) + \Delta x_S(p_i, t_S)) + \nu (x_M(p_0, t_M) + \Delta x_M(p_0, t_M)) \tag{1}$$

of SEVIRI observation $x_S(p_1, t_s)$, $x_S(p_2, t_s)$, ..., $x_S(p_n, t_s)$ made at n different grid
points at time $t_s$ and one MERIS observation $x_M(p_0, t_M)$ at the same pixel ($p_0$), ob-
tained at time $t_M$. $\Delta x_S$ and $\Delta x_M$ denote the SEVIRI and MERIS retrieval error, re-
spectively. The challenge is to determine the optimal weights ($\lambda_1, \ldots, \lambda_n, \nu$) for each
observation. If a time series of $M$ measurements at each location $p_i$ is available, a rea-
sonable requirement is that the mean squared deviation between prediction ($\hat{x}(p_0, t_s)$)
and truth ($x(p_0, t_s)$) is minimal. This leads to a set of ($n + 1$) equations where the sin-
gle terms are covariances between the different measurements, like e.g. the spatial
covariance among the SEVIRI observations, the spatiotemporal covariances between
the MERIS observation and the n SEVIRI measurements and the temporal covariance
between the existing MERIS observations and the collocated prediction point. If the
covariances are known, the weights can be determined and Eq. (1) directly yields the
optimal TCWV estimate at the considered grid point.

In case of the SEVIRI + IASI product, the approach is similar, except that the Kriging
will be performed separately on the vertical layers in order to obtain a merged water
vapour profile. The layered water vapour estimates are obtained by a vertical integra-
tion considering error propagation.

Before the Kriging is applied, systematic differences between the datasets to be
combined are eliminated. Using the monthly means of the individual data, the SEVIRI
bias for each pixel is determined and a bias correction is applied to the 3-hourly SEVIRI

measurements. IASI and MERIS are used as the reference, respectively, because better quality water vapour information compared to SEVIRI is expected from both.

## 4.4.2 Water vapour: results and validation

Important information needed for the Kriging algorithm include the spatial, temporal and spatiotemporal correlations. They are determined on a monthly basis, and examples are shown in Fig. 16 for August 2008. The spatial correlation is determined for SEVIRI and MERIS but due to the better spatial resolution of MERIS, only the MERIS results are used in the following. A spatial correlation length, i.e. the distance where the correlation is decreased to 1/e of its value at zero distance, of about 400 km is found for both instruments. The temporal correlation is based on SEVIRI only, because MERIS observations are not available with sufficient temporal resolution. The temporal correlation length is approximately 19 h. Based on these correlation functions, which are fitted by exponential functions, the spatial, temporal and spatiotemporal correlations between different SEVIRI and MERIS observations are known and the optimal weights in Eq. (1) can be determined. This leads to the merged total column water vapour and an associated uncertainty map. As an example, results for 5 August 2008 12:00–15:00 UTC are displayed in Fig. 17. Compared to the TCWV obtained from SEVIRI only (not shown), the combined product shows a finer spatial structure originating from the MERIS information (overpass at approximately 10:15 UTC).

The validation of the WACMOS water vapour products will be mainly based on comparisons to radiosonde measurements at Global Climate Observing System (GCOS) Upper Air Network (GUAN) stations. In addition, ground-based remote sensing observations from the Meteorological Observatory Lindenberg (MOL), Germany, will be utilised. The water vapour products will also be compared to other satellite based water vapour retrievals, e.g., from Moderate Resolution Imaging Spectroradiometer (MODIS), Advanced TIROS Operational Vertical Sounder (ATOVS), and Special Sensor Microwave Imager (SSM/I).

The AQUA/MODIS total column water vapour (MYD05, collection 5), obtained from the NASA Level 1 and Atmosphere Archive and Distribution System (LAADS), for 5 August 2008 is shown in Fig. 17. Since AQUA passed Central Europe around 12:50 UTC, the MODIS measurements can be compared to the merged SEVIRI + MERIS product in Fig. 17. Three conclusions can be drawn: (1) Some differences in the cloud mask can be observed. (2) The main TCWV structures are very similar. (3) However, higher water vapour amounts are obtained with MODIS. For the selected case, the bias between the SEVIRI + MERIS product and MODIS is $-5\,\mathrm{kg\,m^{-2}}$. Possible reasons for this large bias are currently under investigation. Li et al. (2003) reported that the MODIS near-infrared total column water vapour column appears to overestimate the TCWV compared to radiosonde measurements. Taken into account that MERIS is chosen as a reference for the SEVIRI bias correction, a bias between MODIS and MERIS might be another reason. R. Leinweber (FU Berlin, Germany, personal communication, 2010) finds that MODIS TCWV is $1\text{--}1.5\,\mathrm{kg\,m^{-2}}$ larger than MERIS TCWV over Central Europe based on MERIS data after the 3rd reprocessing. The currently available MERIS data used here uses an older MERIS algorithm (2nd reprocessing) which is known to result in a lower TCWV content than the updated version (R. Leinweber, personal communication, 2010). It can be concluded that the bias to MODIS rather originates from the quality of the retrieval schemes than the combination technique.

## 5  Conclusions

In order to understand the role of the global water cycle in the Earth system it is essential to be able to measure from space hydro-climatic variables, such as radiation, precipitation, evapotranspiration, soil moisture, clouds, water vapour, surface water and runoff, vegetation state, albedo and surface temperature, etc. Such measurements are required to further increase not only our understanding of the different components of the water cycle and its variability, both spatially and temporally, but also to characterise the coupling between the terrestrial and atmospheric branches of the water cycle and

to quantify how this coupling may influence climate variability and predictability. More-over, enhancing the observational capacity and the model capabilities to predict in a reliable manner the variations in the global water cycle will be a key contribution to the improvement of water governance, the mitigation of water-related damages and the
5 sustainable human development.

In the last few years, earth observation has demonstrated the capacity to provide re-liable measurements over oceans, land and atmosphere representing a unique tool for scientist to observe and monitor the earth system. A new era of earth observation has emerged with ever increasing number of missions and sensors available for scientific
10 and operational applications. However, in order to fully exploit this increasing poten-tial and bring this newly available capacity to practical operational levels, significant scientific efforts are required. The Water Cycle Multi-mission Observation Strategy (WACMOS) project is one such effort.

Since the launch of the WACMOS project significant progress has been made with
15 major findings reported in this contribution. The project focuses on developing and validating a novel set of four thematic geo-information products relevant to the wa-ter cycle: evapotranspiration, soil moisture, cloud characterization and water vapour. The generation of these products is based on a number of innovative techniques and methods using multi-mission based strategies to improve current observations thus
20 demonstrating the potential of the synergistic use of the different types of information to be provided by current and future observation systems. In the current phase of the project, emphasis has been on the development of the methodologies and their valida-tion strategies as well as generation of the preliminary demonstration data sets. More specific achievements are summarised as follows:

25 Evapotranspiration: A new parameterization for the ground heat flux is developed for the SEBS algorithm, and a new validation method is proposed using a remote sensing product simulator with the SCOPE model. The system as such is capable to generate turbulent heat fluxes and evapotranspiration using optical and thermal sensors like MERIS and AATSR among others.

Soil moisture: A merged multi-sensor soil moisture climatology is generated for the period 1992–2008 by merging ASCAT and AMSR-E products for the first time. The consistency of the merged product is demonstrated using limited in-situ observations.

Cloud products: The cloud properties generated include Solar Surface Irradiance (SSI) and precipitation occurrence and intensity. Observations from the SEVIRI instrument are combined with water vapour profiles from the MERIS instrument to obtain these cloud properties at regional scale and at high temporal resolution at every hour or even every 15 min. Observations from polar orbiting instrument SCIAMACHY are used to derive SSI and Condensed Water Path (CWP) at global scale.

Water vapour: For the first time SEVIRI and MERIS instruments have been successfully combined into a water vapour product using a geostaistical approach. Systematic deviations between the combined product and other (MODIS) satellite products are noticed which are caused by differences in the cloud mask and the individual retrieval schemes rather than the combination methodology.

Despite these preliminary important achievements, it is evident that the production of global water cycle products fulfilling the GCOS ECVs requirements will require substantially bigger efforts. It is strategically important and opportune to continue and intensify the present efforts such that the developed methodologies and the validation strategies can be further applied to reprocessed satellite data records to generate global water cycle products for the improvement of water governance, the mitigation of water-related damages and the sustainable human development. Further information and details of data products can be obtained at the website wacmos.org.

**Earth observation Water Cycle Multi-Mission Observation Strategy**

Z. Su et al.

Title Page

| Abstract | Introduction |
| Conclusions | References |
| Tables | Figures |

◄◄ ►►

◄ ►

Back Close

Full Screen / Esc

Printer-friendly Version

Interactive Discussion

# References

Anderson, M. C., Norman, J. M., Kustas, W. P., Houborg, R., Starks, P. J., and Agam, N.: A thermal-based remote sensing technique for routine mapping of land-surface carbon, water and energy fluxes from field to regional scales, Remote Sens. Environ., 112, 4227–4241, 2008.

Baldocchi, D., Falge, E., Gu, L. H., Olson, R., Hollinger, D., Running, S., Anthoni, P., Bernhofer, C., Davis, K., Evans, R., Fuentes, J., Goldstein, A., Katul, G., Law, B., Lee, X. H., Malhi, Y., Meyers, T., Munger, W., Oechel, W., Pilegaard, K., Schmid, H. P., Valentini, R., Verma, S., Vesala, T., Wilson, K., and Wofsy, S.: FLUXNET: A new tool to study the temporal and spatial variability of ecosystem-scale carbon dioxide, water vapor, and energy flux densities, B. Am. Meteorol. Soc., 82, 2415–2434, 2001.

Bartalis, Z., Wagner, W., Naeimi, V., Hasenauer, S., Scipal, K., Bonekamp, H., Figa, J., and Anderson, C.: Initial soil moisture retrievals from the METOP-A Advanced Scatterometer (ASCAT), Geophys. Res. Lett., 34, L20401, doi:10.1029/2007GL031088, 2007.

Bastiaanssen, W. G. M., Menenti, M., Feddes, R. A., and Holtslag, A. A. M.: A remote sensing surface energy balance algorithm for land (SEBAL), 1. Formulation, J. Hydrol., 212–213, 198–212, 1998.

Bengtsson, L.: The global atmospheric water cycle, Environ. Res. Lett., 5, 1–8, doi:10.1088/1748-9326/5/2/025002, 2010.

Bowen, I. S.: The ratio of heat losses by conduction and by evaporation from any water surface, Phys. Rev., 27, 779–787, 1926.

Brutsaert, W.: Aspects of Bulk Atmospheric Boundary Layer Similarity Under Free-Convective Conditions, Rev. Geophys., 37, 439-451, 1999.

CEOS: The earth observation handbook, www.eohandbook.com, last access: 8 October 2010, 2009.

Deneke, H. M., Feijt, A. J., and Roebeling, R. A.: Estimating surface solar irradiance from METEOSAT SEVIRI-derived cloud properties, Remote Sens. Environ., 112, 3131–3141, doi:10.1016/j.rse.2008.03.012, 2008.

Deneke, H. M. and Roebling, R.: Downscaling of METEOSAT SEVIRI 0.6 and 0.8 micron channel radiances utilizing the high-resolution visible channel, Atmos. Chem. Phys. Discuss., 10, 10707–10740, doi:10.5194/acpd-10-10707-2010, 2010.

Title Page

Abstract | Introduction

Conclusions | References

Tables | Figures

Back | Close

Full Screen / Esc

Printer-friendly Version

Interactive Discussion

Derrien, M. and LeGléau, H.: MSG/SEVIRI cloud mask and type from SAFNWC, Int. J. Remote Sens., 26, 4707–4732, 2005.

Dorigo, W. A., Scipal, K., Parinussa, R. M., Liu, Y. Y., Wagner, W., de Jeu, R. A. M., and Naeimi, V.: Error characterisation of global active and passive microwave soil moisture data sets, Hydrol. Earth Syst. Sci. Discuss., 7, 5621–5645, doi:10.5194/hessd-7-5621-2010, 2010.

Drusch, M., Wood, E. F., and Gao, H.: Observation operators for the direct assimilation of TRMM microwave imager retrieved soil moisture, Geophys. Res. Lett., 32, L15403, doi:10.1029/2005GL023623, 2005.

Entekhabi, D., Njoku, E., Houser, P., Spencer, M., Doiron, T., Smith, J., Girard, R., Belair, S., Crow, W., Jackson, T., Kerr, Y., Kimball, J., Koster, R., McDonald, K., O'Neill, P., Pultz, T., Running, S., Shi, J. C., Wood, E., and van Zyl, J.: The Hydrosphere State (HYDROS) mission concept: An Earth system pathfinder for global mapping of soil moisture and land freeze/thaw, IEEE T. Geosci. Remote, 42(10), 2184–2195, , 2004.

ESA: EarthCARE – Earth Clouds, Aerosols and Radiation Explorer, http://esamultimedia.esa.int/docs/SP_1279_1_EarthCARE.pdf, last access: 8 October 2010, ESA SP-1279(1), 66 pp., 2004.

ESA: The changing earth, http://esamultimedia.esa.int/docs/SP-1304.pdf, last access: 8 October 2010, ESA SP-1304, 85 pp., 2006.

EUMETSAT Satellite Application Facility on Nowcasting and Very Short Range Forecasting: Algorithm Theoretical Basis Document for PGE13 "SEVIRI Physical Retrieval Product" (SPhR) v1.0, 2010.

Famiglietti, J. S. and Wood, E. F.: Multiscale modeling of spatially variable water and energy balance processes, Water Resour. Res., 30, 3061–3078, 1994.

Fischer, J. and Bennartz, R.: MERIS Algorithm Theoretical Basis Document (ATBD 2.4), Retrieval of total water vapour content from MERIS measurements, 1997.

GCOS: Implementation plan for the Global Observing System for climate in support of the UNFCC (2010 Update), http://www.wmo.int/pages/prog/gcos/Publications/gcos-138.pdf' last access: 8 October 2010, GCOS-138, 180 pp., 2010.

GEO: GEOSS, 10-Year Implementation Plan, Reference Document, GEO 1000R, 73 pp., 2005.

GEO: The full picture, http://www.earthobservations.org/documents/the_full_picture.pdf last access: 8 October 2010, 2007.

Glenn, E. P., Huete, A. R., Nagler, P. L., Hirschboeck, K. K., and Brown, P.: Integrating remote sensing and ground methods to estimate evapotranspiration, Crit. Rev. Plant Sci., 26, 139–168, 2007.

Held, I. and Soden, B.: Water vapor feedback and global warming, Ann. Rev. Energ. Env., 25, 441–475, 2000.

IPCC: Technical Paper on climate change and water, IPCC, April, 2008.

Jackson, T. J., Vine, D. M. L., Hsu, A. Y., Oldack, A., Starks, P. J., Swift, C. T., Isham, J. D., and Haken, M.: Soil moisture Mapping at regional scales using microwave radiometry: The Southern Great Plins hydrology experiment, IEEE T. Geosci. Remote, 37, 2136–2149, 1999.

Kalma, J. D., McVicar, T. R., and McCabe, M. F.: Estimating Land Surface Evaporation: A Review of Methods Using Remotely Sensed Surface Temperature Data, Surv. Geophys. 29, 421–469, 2008.

Kerr, Y., Waldteufel, P., Wigneron, J. P., Martinuzzi, J. M., Font, J., and Berger, M.: Soil moisture retrieval from space: The Soil Moisture and Ocean Salinity (SMOS) mission, IEEE T. Geosci. Remote, 39(8), 1729–1735, 2001.

Kite, G. W. and Droogers, P.: Comparing evapotranspiration estimates from satellites, hydrological models and field data, J. Hydrol., 229, 3–18, 2000.

Kolmogorov, A. N.: The Local Structure of Turbulence in Incompressible Viscous Fluid for Very Large Reynolds Numbers, Proc. Math. Phys. Sc., 434, 9–13, 1991.

Kustas, W. P. and Norman, J. M.: A Two-Source Energy Balance Approach Using Directional Radiometric Temperature Observations for Sparse Canopy Covered Surfaces, Agron. J., 92, 847–854, 2000.

Li, Z., Muller, J. P., and Cross, P.: Comparison of precipitable water vapor derived from radiosonde, GPS, and moderate-resolution imaging spectroradiometer measurements, J. Geophys. Res., 108(D20), 4651, doi:10.1029/2003JD003372, 2003.

Lindenbergh, R., Keshin, M., van der Marel, H., and Hanssen, R.: High resolution spatiotemporal water vapour mapping using GPS and MERIS observations, Int. J. Remote Sens., 29(8), 2393–2409, 2008.

Liu, Y. Y., Parinussa, R. M., Dorigo, W. A., de Jeu, R. A. M., Wagner, W., van Dijk, A. I. J. M., McCabe, M. F., and Evans, J. P.: Developing an improved soil moisture dataset by blending passive and active microwave satellite-based retrievals, Hydrol. Earth Syst. Sci. Discuss., 7, 6699–6724, doi:10.5194/hessd-7-6699-2010, 2010.

Title Page

Abstract | Introduction

Conclusions | References

Tables | Figures

◄ | ►

◄ | ►

Back | Close

Full Screen / Esc

Printer-friendly Version

Interactive Discussion

Liu, Y. Y., Van Dijk, A. I. J. M., De Jeu, R. A. M., and Holmes, T. R. H.: An analysis of spatiotemporal variations of soil and vegetation moisture from a 29-year satellite-derived data set over mainland Australia, Water Resour. Res., 45, W07405, doi:10.1029/2008WR007187, 2009.

Mazvimavi, D. and Wolski, P.: Long-term variations of annual flows of the Okavango and Zambezi Rivers, Phys. Chem. Earth, 31, 944–951, 2006.

MERIS PQSR: MERIS Products Quality Status Report, Issue: Version 1, Prepared by the MERIS Quality Working Group, 14 March, 2006.

Minnis, P., Garber, D. P., Young, D. F., Arduini, R. F., and Takano, Y.: Parameterizations of Reflectance and Effective Emittance for Satellite Remote Sensing of Cloud Properties, J. Atmos. Sci., 55, 3313–3339, 1998.

Miralles, D. G., Crow, W. T., and Cosh, M. H.: Estimating spatial sampling errors in coarse-scale soil moisture estimates derived from point-scale observations, J. Hydrometeorol., in review, 2010.

Monin, A. S. and Obukhov, A. M.: Osnovnye zakonomernosti turbulentnogo peremesivanija v prizemnom sloe atmosfery, Trudy geofiz. inst. AN SSSR 24 (151), 163–187, 1954.

Monteith, J. L.: Evaporation and the environment, in: Symposium of the society for experimental biology, 19(2965), 203–234, 1965.

Müller, R., Matsoukas, C., Gratzki, A., Hollmann, R., and Behr, H.: The CM-SAF operational scheme for the satellite based retrieval of solar surface irradiance – a lut based eigenvector hybrid approach, Remote Sens. Environ., 113(5), 1012–1024, 2009.

Nakajima, T. and King, M. D.: Determination of the optical thickness and effective particle radius of clouds from reflected solar radiation measurements, Part I. Theory, J. Atmos. Sci., 47, 1878–1893, 1990.

Njoku, E. G., Jackson, T. J., Lakshmi, V., Chan, T. K., and Nghiem, S. V.: Soil moisture retrieval from AMSR-E, IEEE T. Geosci. Remote, 41, 215–229, 2003.

Obukhov, A. M.: Turbulence in an atmosphere with a non-uniform temperature, Bound.-Lay. Meteorol., 2, 7–29, 1971.

Owe, M., De Jeu, R., and Holmes, T.: Multisensor historical climatology of satellite-derived global land surface moisture, J. Geophys. Res.-Earth, 113, F01002, doi:10.1029/2007JF000769, 2008.

Pauwels, V. R. N. and Samson, R.: Comparison of different methods to measure and model actual evapotranspiration rates for a wet sloping grassland, Agr. Water Manage., 82, 1–24, 2006.

Title Page

Abstract | Introduction

Conclusions | References

Tables | Figures

◀◀ | ▶▶

◀ | ▶

Back | Close

Full Screen / Esc

Printer-friendly Version

Interactive Discussion

Pauwels, V. R. N., Timmermans, W., and Loew, A.: Comparison of the estimated water and energy budgets of a large winter wheat field during AgriSAR 2006 by multiple sensors and models, J. Hydrol., 349, 425–440, 2008.

Penman, H. L.: Natural evaporation from open water, bare soil and grass, P. Roy. Soc. A, 193, 120–146, 1948.

Roebeling, R. A. and Holleman, I.: Development and validation of rain rate retrievals from SEVIRI using weather radar observations, J. Geophys. Res., 114, D21202, doi:10.1029/2009JD012102, 2009.

Roebeling, R. A., Feijt, A. J., and Stammes, P.: Cloud property retrievals for climate monitoring: implications of differences between SEVIRI on METEOSAT-8 and AVHRR on NOAA-17, J. Geophys. Res., 11, D20210, doi:10.1029/2005JD006990, 2006.

Schulz, J., Albert, P., Behr, H.-D., Caprion, D., Deneke, H., Dewitte, S., Dürr, B., Fuchs, P., Gratzki, A., Hechler, P., Hollmann, R., Johnston, S., Karlsson, K.-G., Manninen, T., Müller, R., Reuter, M., Riihelä, A., Roebeling, R., Selbach, N., Tetzlaff, A., Thomas, W., Werscheck, M., Wolters, E., and Zelenka, A.: Operational climate monitoring from space: the EUMETSAT Satellite Application Facility on Climate Monitoring (CM-SAF), Atmos. Chem. Phys., 9, 1687–1709, doi:10.5194/acp-9-1687-2009, 2009.

Scipal, K., Holmes, T., De Jeu, R., Naeimi, V., and Wagner, W.: A possible solution for the problem of estimating the error structure of global soil moisture data sets, Geophys. Res. Lett., 35, L24403, doi:10.1029/2008GL035599, 2008.

Stammes, P.: Spectral radiance modeling in the UV-Visible range, in: IRS 2000: Current problems in Atmospheric Radiation, edited by: Smith, W. L. and Timofeyev, Y. M., A. Deepak Publ., Hampton, Va., 385–388, 2001.

Stamnes, K., Tsay, S., Wiscombe, W., and Jayaweera, K.: Numerically stable algorithm for discrete-ordinate-method radiative transfer in multiple scattering and emitting layered media, Appl. Optics, 27, 2502–2509, 1988.

Su, Z.: Observation of hydrological processes using remote sensing, in Treatise on Water Science, Volume 2, Chapter 42, Hydrology, Elsevier, in press, 2010.

Su, Z., Schmugge, T., Kustas, W. P., and Massman, W. J.: An evaluation of two models for estimation of the roughness height for heat transfer between the land surface and the atmosphere, J. Appl. Meteorol., 40, 1933–1951, 2001.

Su, Z.: The Surface Energy Balance System (SEBS) for estimation of turbulent heat fluxes, Hydrol. Earth Syst. Sci., 6, 85–100, doi:10.5194/hess-6-85-2002, 2002.

Title Page

Abstract | Introduction

Conclusions | References

Tables | Figures

◀ | ▶

◀ | ▶

Back | Close

Full Screen / Esc

Printer-friendly Version

Interactive Discussion

Su, Z., Wen, J., and Wagner, W.: Preface "Advances in land surface hydrological processes - field observations, modeling and data assimilation", Hydrol. Earth Syst. Sci., 14, 365–367, doi:10.5194/hess-14-365-2010, 2010.

Timmermans, J., Van der Tol, C., Verhoef, A., Verhoef, W., Su, Z., van Helvoirt, M., and Wang, L.: Quantifying the uncertainty in estimates of surface atmosphere fluxes by evaluation of SEBS and SCOPE models, Hydrol. Earth Syst. Sci. Discuss., submitted, 2010.

Trenberth, K. E. and Stepaniak, D. P.: Co-variability of components of poleward atmospheric energy transports on seasonal and interannual timescales, J. Climate, 16, 3690–3704, 2003.

van der Tol, C., van der Tol, S., Verhoef, A., Su, B., Timmermans, J., Houldcroft, C., and Gieske, A.: A Bayesian approach to estimate sensible and latent heat over vegetated land surface, Hydrol. Earth Syst. Sci., 13, 749–758, doi:10.5194/hess-13-749-2009, 2009a.

van der Tol, C., Verhoef, W., Timmermans, J., Verhoef, A., and Su, Z.: An integrated model of soil-canopy spectral radiances, photosynthesis, fluorescence, temperature and energy balance, Biogeosciences, 6, 3109–3129, doi:10.5194/bg-6-3109-2009, 2009b.

Verhoef, A., McNaughton, K. G., and Jacobs, A. F. G.: A parameterization of momentum roughness length and displacement height for a wide range of canopy densities, Hydrol. Earth Syst. Sci., 1, 81–91, doi:10.5194/hess-1-81-1997, 1997.

Verhoef, W., Jia, L., Xiao, Q., and Su, Z.: Unified optical-thermal four-stream radiative transfer theory for homogeneous vegetation canopies, IEEE T. Geosci. Remote, 45, 1808–1822, 2007.

Wagner, W., Lemoine, G., and Rott, H.: A method for estimating soil moisture from ERS scatterometer and soil data, Remote Sens. Environ., 70, 191–207, 1999.

Wagner, W., Verhoest, N. E. C., Ludwig, R., and Tedesco, M.: Editorial "Remote sensing in hydrological sciences", Hydrol. Earth Syst. Sci., 13, 813–817, doi:10.5194/hess-13-813-2009, 2009.

Wang, P., Stammes, P., van der A, R., Pinardi, G., and van Roozendael, M.: FRESCO+: an improved $O_2$ A-band cloud retrieval algorithm for tropospheric trace gas retrievals, Atmos. Chem. Phys., 8, 6565–6576, doi:10.5194/acp-8-6565-2008, 2008.

WMO/GCOS: Systematic Observation Requirements for Satellite-based Products for Climate – Supplemental details to the satellite-based component of the Implementation Plan for the Global Observing System for Climate in Support of the UNFCCC, GCOS-107, WMO/TD. No 1338, September, 2006.

Title Page

Abstract | Introduction

Conclusions | References

Tables | Figures

◄ | ►|

◄ | ►

Back | Close

Full Screen / Esc

Printer-friendly Version

Interactive Discussion

WMO/ReqObs: Requirements for observations for global NWP, WMO, Expert team on observational data requirements and redesign of the global observing system, Reference Number CBS/OPAG-IOS, ODRRGOS-4/INF. 4, 11 October, 2001.

Wolters, E. L. A., Roebeling, R. A., and Feijt, A. J.: Evaluation of cloud phase retrieval methods for SEVIRI onboard METEOSAT-8 using ground-based lidar and cloud radar data, J. Appl. Meteorol. Clim., 47(6), 1723–1738, doi:10.1175/2007JAMC1591.1, 2008.

Wolters, E. L. A., van den Hurk, B. J. J. M., and Roebeling, R. A.: Rainfall retrievals over West Africa using SEVIRI: evaluation with TRMM-PR and monitoring of the daylight time monsoon progression, Hydrol. Earth Syst. Sci. Discuss., 7, 6351–6380, doi:10.5194/hessd-7-6351-2010, 2010.

Young, R., Walker, J., Yeoh, N., Smith, A., Ellett, K., Merlin, O., and Western, A.: Soil moisture and meteorological observations from the murrumbidgee catchment, Department of Civil and Environmental Engineering, The University of Melbourne, 2008.

**Table 1.** Overview of WACMOS product properties. Spatial resolution at nadir is given in km$^2$. Codes for temporal resolution are: H = hourly value, D = daily mean and M = monthly mean. Codes for areas are: MD = MSG disc and GC = global coverage.

| Product group | Product name | Sensor | Area | Spatial and temporal resolution | Accuracy (bias) and Precision (RMSE) | Unit |
|---|---|---|---|---|---|---|
| Evapotrans-piration | ET, HR<br>ET, LR | AATSR, MERIS, MODIS, MSG | MD<br>GC | $1 \times 1\,km^2$, D<br>$25 \times 25\,km^2$, D | 25% (uncerantity on land/ocean)<br>25% (uncerantity on land/ocean) | mm |
| Soil moisture | SOILM | AMSR-E, Windsat, TRMM, SSM/I, SMMR, ERS 1-2, ASCAT | GC | 0.25° grid, D | 0.04–0.08 depending on land cover (Variable) | $m^3\,m^{-3}$ |
| Clouds | SSI<br>SSI<br>PRECIP<br>CWP | SEVIRI<br>SCIAMACHY<br>SEVIRI<br>SCIAMACHY | MD<br>GC<br>MD<br>GC | $3 \times 3\,km^2$, H<br>$30 \times 60\,km^2$, D<br>$3 \times 3\,km^2$, H<br>$32 \times 215\,km^2$, D | 5 (25)<br>5 (100)<br>0.1 (1.0)<br>20 (40) | $W\,m^{-2}$<br>$W\,m^{-2}$<br>$mm\,h^{-1}$<br>$g\,m^{-2}$ |
| Water Vapour | WV<br><br>WV | SEVIRI + IASI<br><br>SEVIRI + MERIS | MD<br><br>NE Europe | $(0.25°)^2$, 3H<br><br>$(0.025°)^2$, 3H | 0.2 (0.8), 0.6 (2.0), 0.8 (3.0) (for top, middle and bottom layer)<br>1 (4) | $kg\,m^{-2}$<br><br>$kg\,m^{-2}$ |

Title Page

Abstract | Introduction

Conclusions | References

Tables | Figures

◀◀ | ▶▶

◀ | ▶

Back | Close

Full Screen / Esc

Printer-friendly Version

Interactive Discussion

**Table 2.** SEBS variable dependence on Remote Sensing Products.

| SEBS required Variables | AATSR/MERIS | | MSG | |
|---|---|---|---|---|
| | product name | Temp. Res. | product name | Temp. Res. |
| Height of canopy | -> MER_RR__2P | Swath dep. | -> NDVI | Daily |
| LAI | -> MER_RR__2P | Swath dep. | LSA SAF LAI | Daily |
| Fraction. Veg. Cov. | -> MER_RR__2P | Swath dep. | LSA SAF HC | Daily |
| Albedo | -> MER_RR__2P | Swath dep. | LSA SAF Albedo | Daily |
| Emissivity | -> NDVI | Swath dep. | -> NDVI | Daily |
| LST | ATS_NR__2P | Swath dep. | LSA SAF LST | 30 min |
| NDVI | ATS_NR__2P | Swath dep. | -> L2 data | Daily |
| SWd | – | – | DSSF | 30 min |
| LWd | – | – | DSLF | 30 min |

**Table 3.** SEBS variable dependence on ECMWF data. For certain conditions the boundary layer height can become lower than the lowest height level – hpbl < min(zlevel). In that case the algorithm uses variables estimated at surface level height.

| SEBS Inputs | | Product level | Variable |
|---|---|---|---|
| SWd | | Surface var. | Surface solar radiation downwards |
| LWd | | Surface var. | Surface thermal radiation downwards |
| Tdew | | Pressure levels var. | 02 meter dew temperature |
| P0 | | Surface var. | Mean sea level pressure |
| Ps | | Surface var. | Surface pressure |
| Hpbl | | Surface var. | Boundary layer height |
| Pref | | Pressure levels var. | Pressure Levels |
| Geopotential height | | Pressure levels var. | Geopotential |
| Zlevels | | Levels + Geopotential height | Height level |
| Tair | hpbl < min(zlevel) | Surface var. | 02 meter temperature |
| | hpbl => min(zlevel) | Pressure levels var. | Temperature |
| Wind speed | hpbl < min(zlevel) | Surface var. | 10 m $V+U$ wind speed |
| | hpbl => min(zlevel) | Pressure levels var. | $V+U$ wind speed |
| $Q$ | hpbl < min(zlevel) | – | Tair + Tdew + Ps |
| | hpbl => min(zlevel) | Pressure levels var. | Specific Humidity |
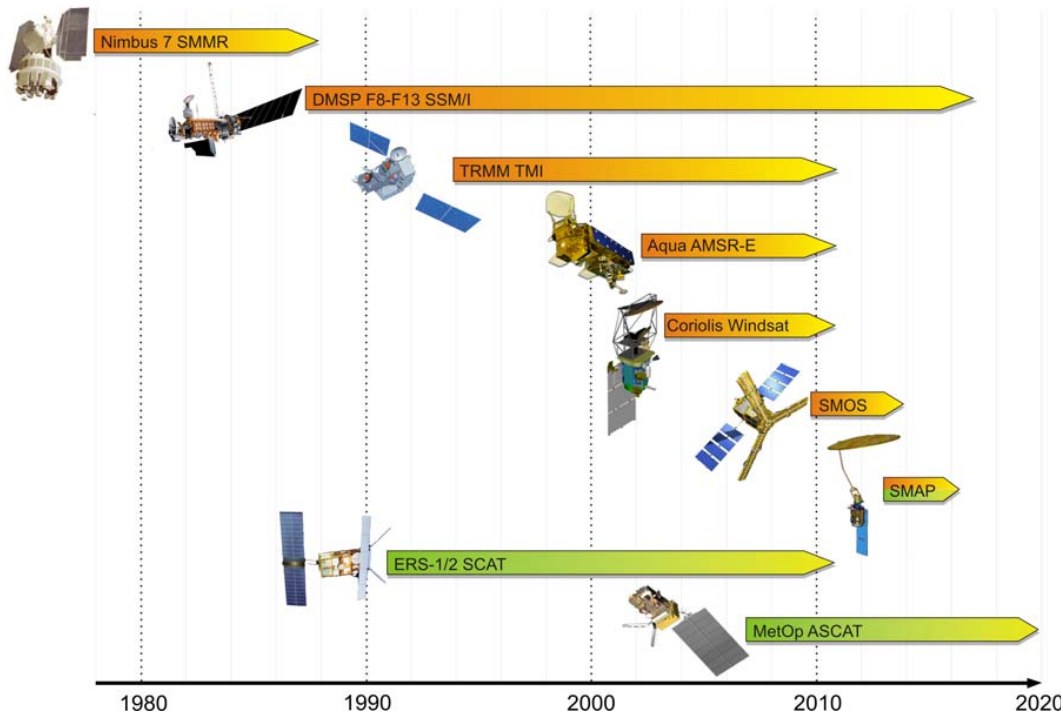
**Fig. 1.** Time line of past, current, and future spaceborne coarse resolution radiometers (orange) and scatterometers (green) suited for soil moisture retrieval on a global scale.

Full Screen / Esc

Printer-friendly Version

Interactive Discussion
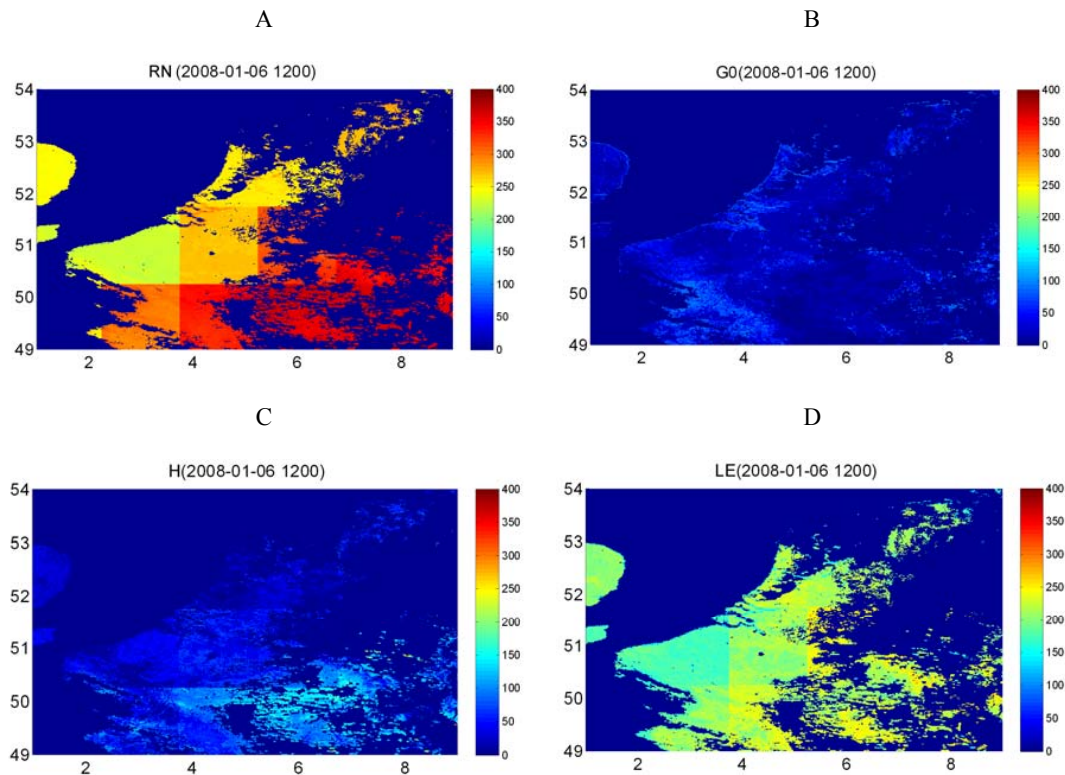
**Fig. 2.** Surface Heat fluxes over the Netherlands on 6 January 2008, from MODIS level 2 products. The net radiation, soil heat flux, sensible heat flux and latent heat flux is shown in respectively figure **(A)**, **(B)**, **(C)**, **(D)**.

Title Page

Abstract        Introduction

Conclusions     References

Tables          Figures

|◄              ►|

◄               ►

Back            Close

Full Screen / Esc

Printer-friendly Version

Interactive Discussion
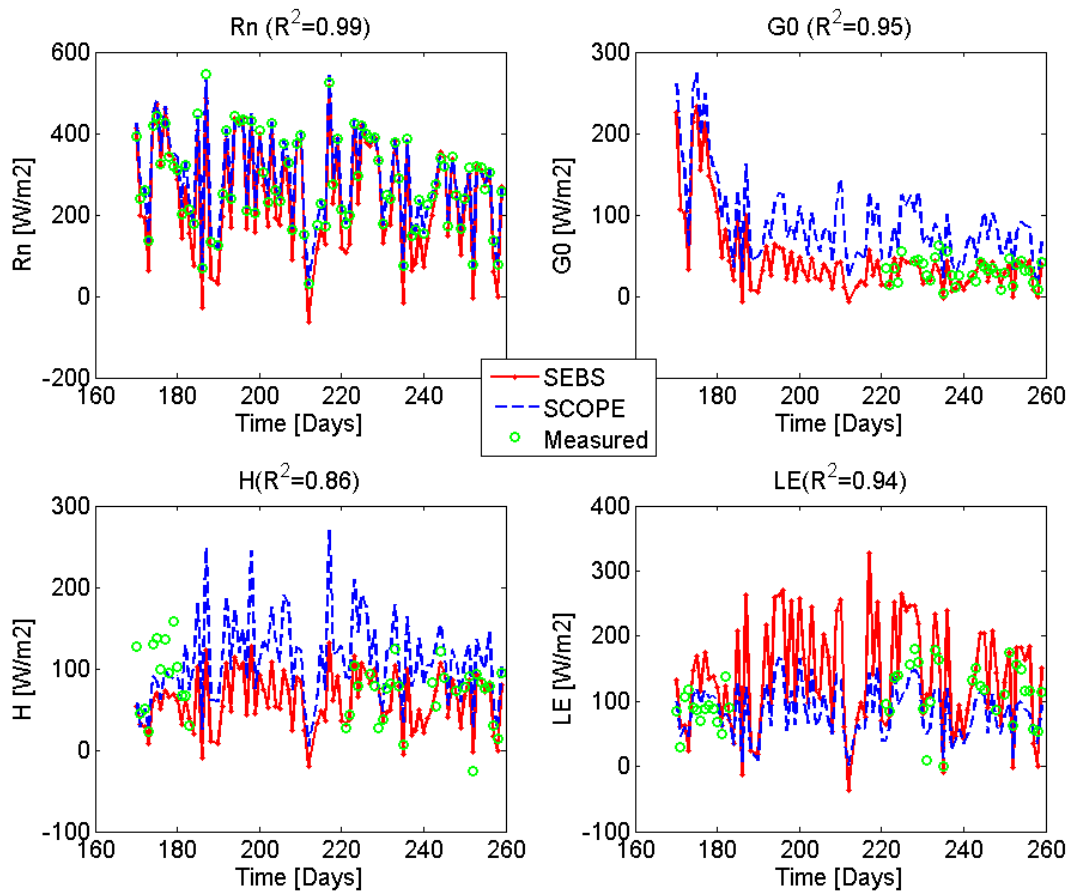
**Fig. 3.** Time series of actual surface heat fluxes obtained from field measurements and obtained using SEBS and SCOPE. The data was acquired over the Sonning Site, Reading, the UK in 2008. The correlation between SEBS and SCOPE is provided for each surface heat flux.
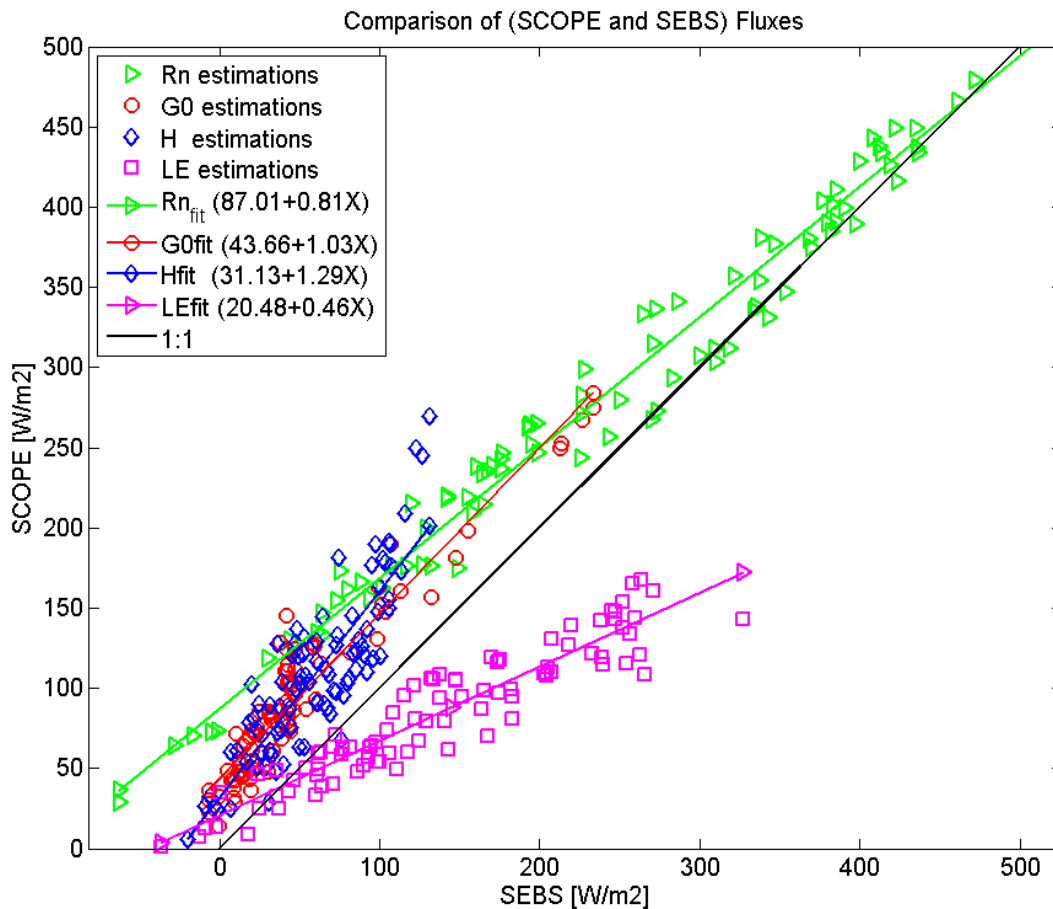
**Fig. 4.** Correlations between SEBS and SCOPE surface heat fluxes. The data was acquired over the Sonning Site, Reading, the UK in 2008.

Title Page

Abstract | Introduction

Conclusions | References

Tables | Figures

|◄ | ►|

◄ | ►

Back | Close

Full Screen / Esc

Printer-friendly Version

Interactive Discussion
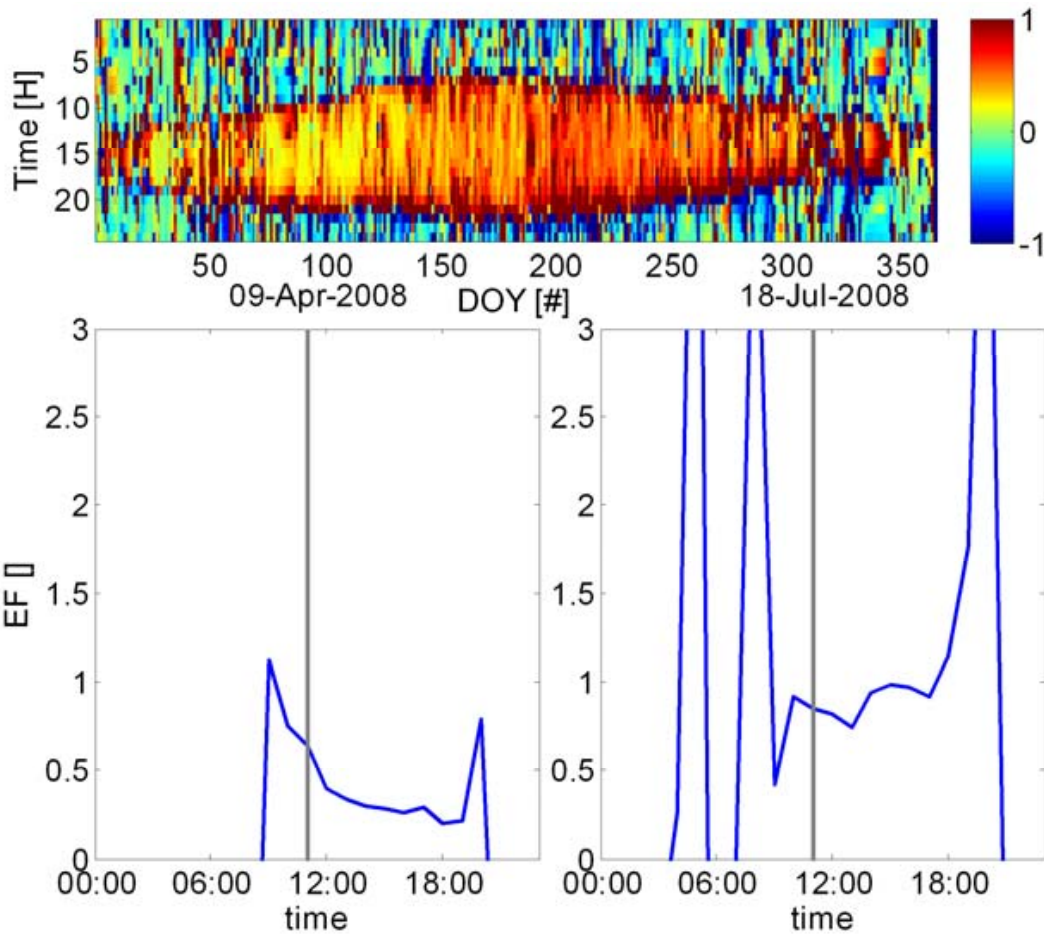
**Fig. 5.** Daily evaporative fraction over the Speulder forest, Garderen, the Netherlands.

Title Page

Abstract    Introduction

Conclusions    References

Tables    Figures

Back    Close

Full Screen / Esc

Printer-friendly Version

Interactive Discussion
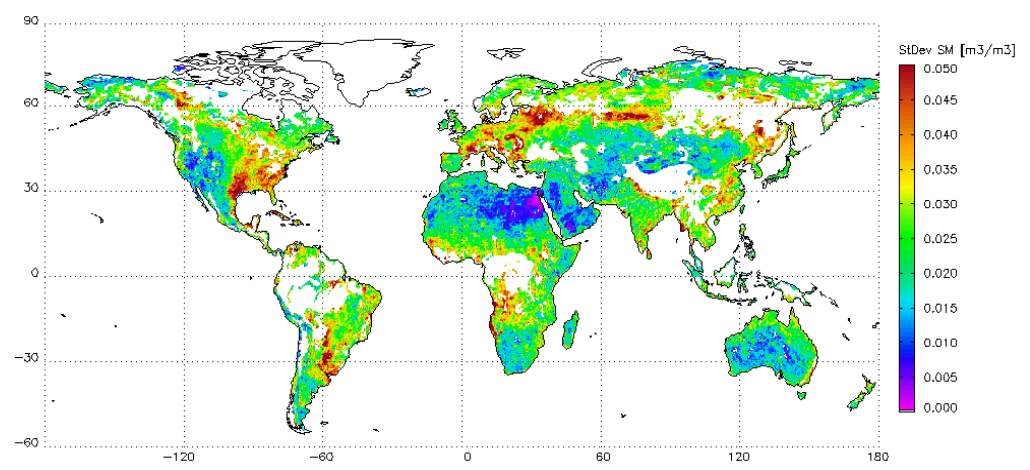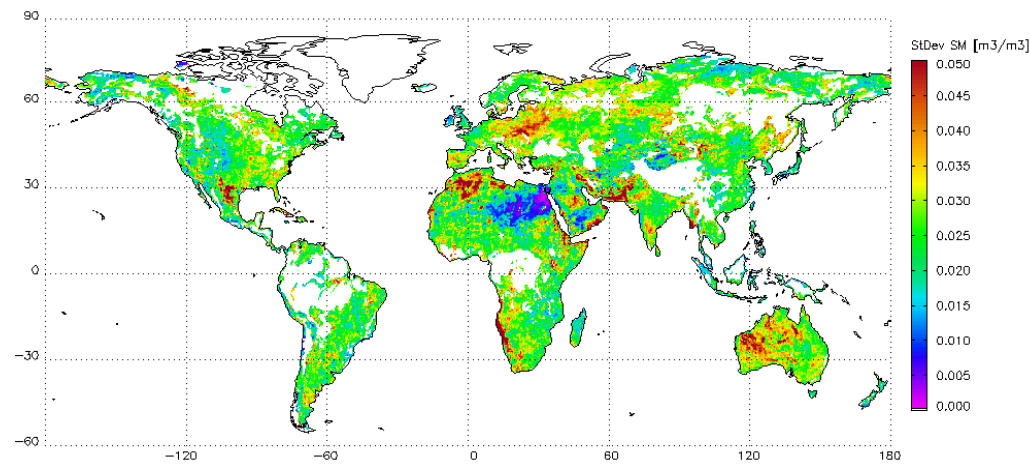
**Fig. 6.** Spatial errors of derived soil moisture estimates (mm) of ASCAT (above) and AMSR-E (below). White areas on the land surface indicate regions with less than 100 triplets.

Title Page

Abstract | Introduction

Conclusions | References

Tables | Figures

◀ | ▶|

◀ | ▶

Back | Close

Full Screen / Esc

Printer-friendly Version

Interactive Discussion
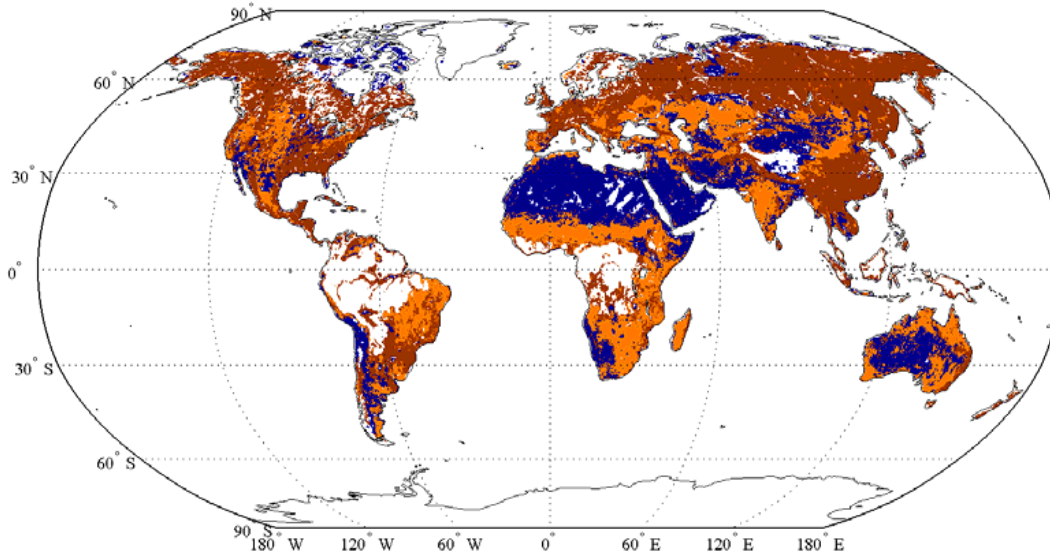
**Fig. 7.** Spatial coverage of areas where only observations of AMSR-E (blue), only ASCAT (red) or both data sets (orange) are used for the merged product.
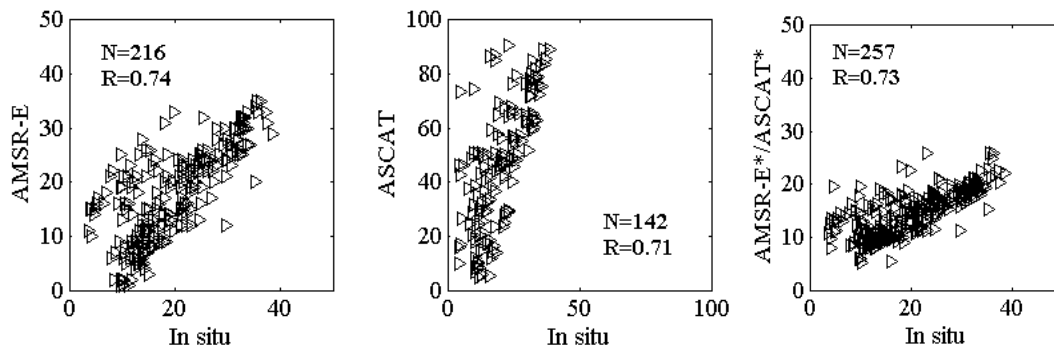
**Fig. 8.** Relationship between satellite-based soil moisture estimates and in-situ measurements from the OzNet network for a location in southeast Australia. The left and middle graphs show the results for the original AMSR-E and ASCAT products, the right graph those of the merged and rescaled product.

Full Screen / Esc

Printer-friendly Version

Interactive Discussion
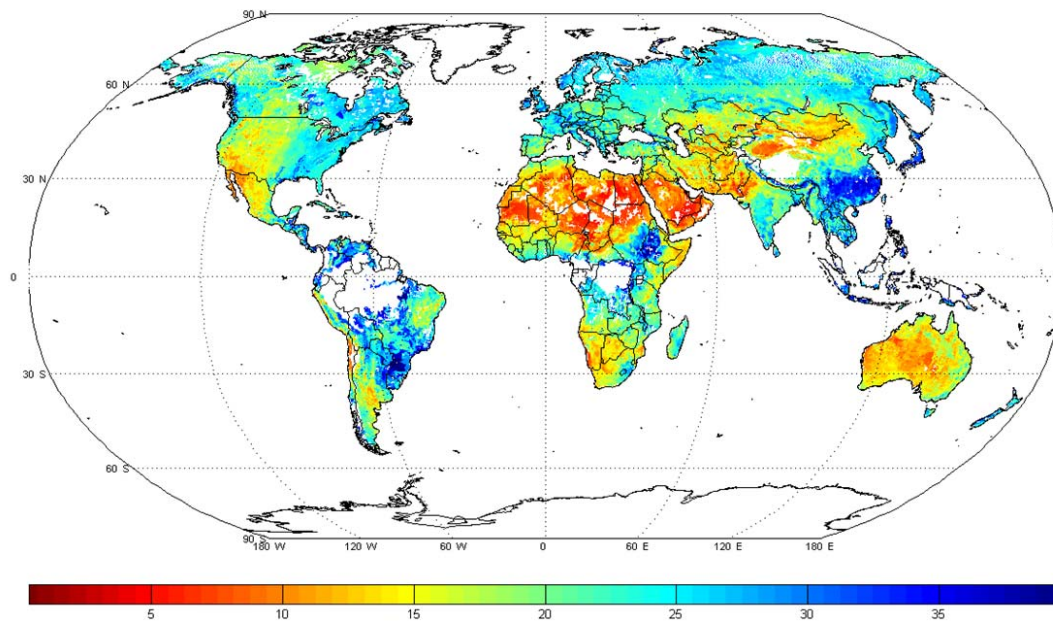


**Fig. 9.** Average soil moisture content (%) calculated from multi-sensor (active + passive) soil moisture climatology (1992–2008).
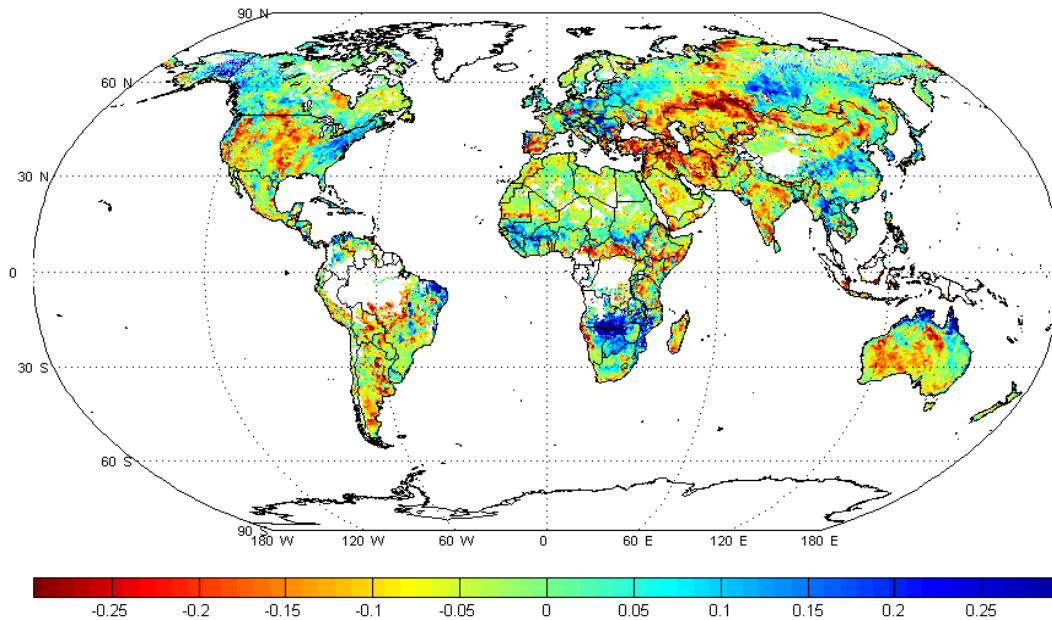
**Fig. 10.** Average yearly change in soil moisture content (%) over the period 1992–2008, calculated from the merged multi-sensor soil moisture data set.
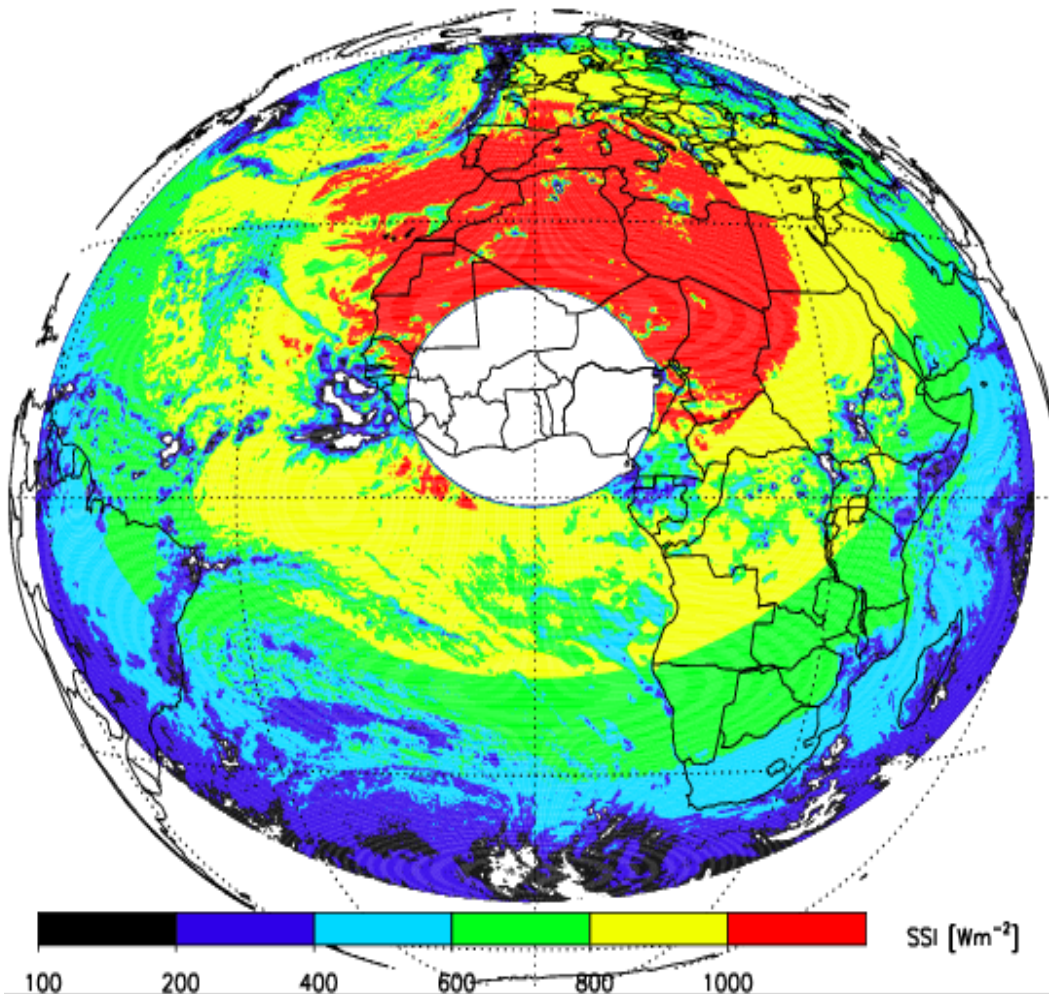
**Fig. 11.** Example of instantaneous MSG-SEVIRI SSI products for 1 July 2008 at 12:00 UTC.
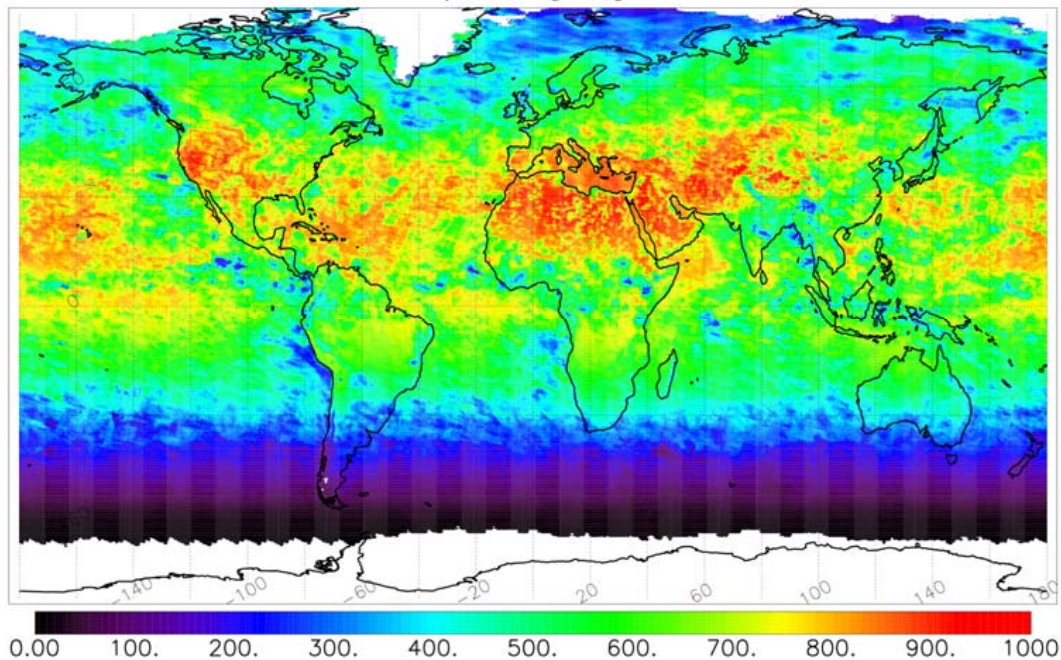
**Fig. 12.** Example of the global mean SSI in W m$^{-2}$ from SCIAMACHY for July 2008.

**Fig. 13.** Example monthly mean precipitation occurrence (left panel) and intensity (right panel) product for July 2008. Note that these products were calculated from daytime observations between 6 and 18 h.
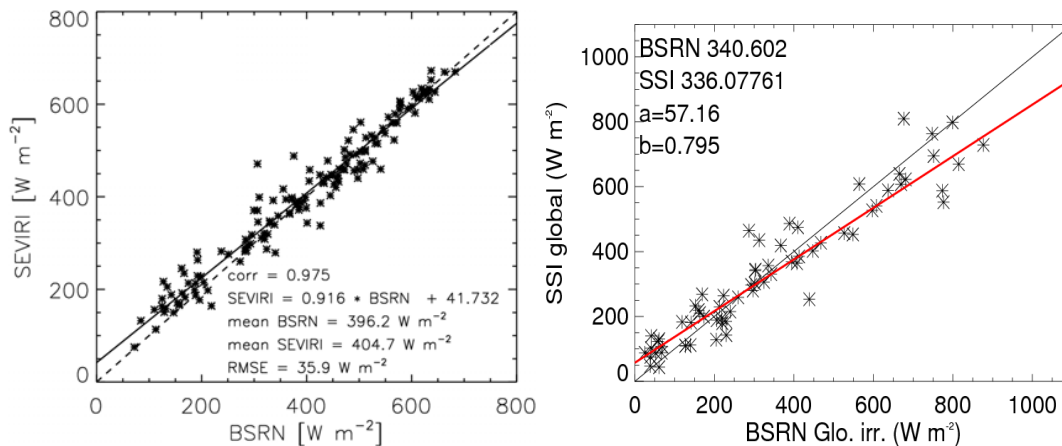
**Fig. 14.** Comparison of solar surface irradiance retrieved from SEVIRI cloud physical properties (left panel) and from SCIAMACHY effective cloud fraction (right panel) against BSRN observations taken at Cabauw, the Netherlands. The SEVIRI retrievals represent daily mean values during May–September 2008 while the SCIAMACHY values represent observation taken approximately once every six days during 2008.
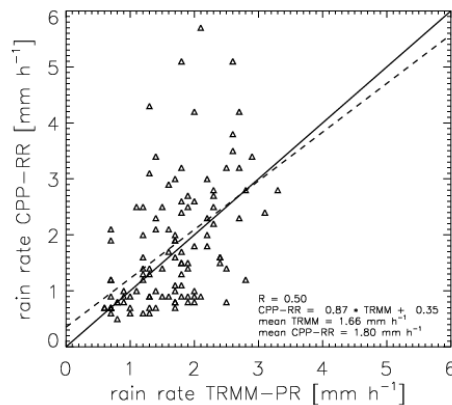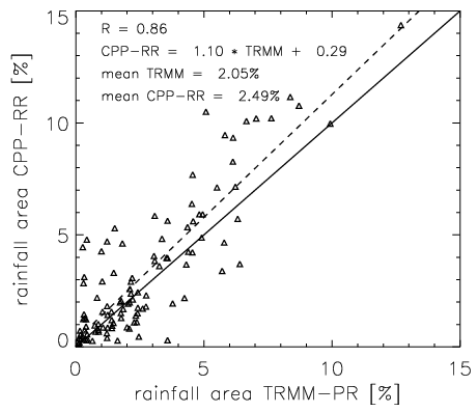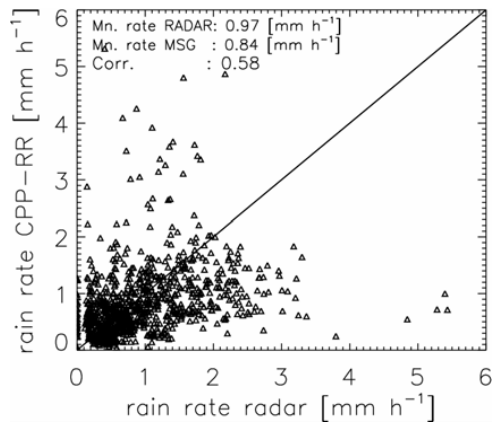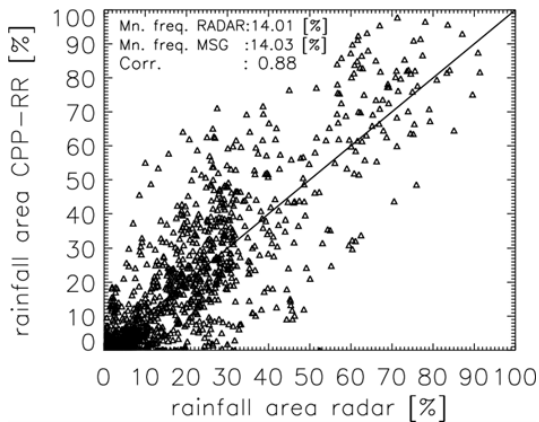
**Fig. 15.** Scatter plots of SEVIRI retrieved versus reference instrument observed areal mean precipitation occurrences (left panels) and rain rates (right panels). The upper panel shows the plots of CPP-RR versus weather radar for central Europe. The lower panel shows the plots of CPP-RR versus TRMM-PR for Western Africa.

Title Page

Abstract | Introduction

Conclusions | References

Tables | Figures

|◄ | ►|

◄ | ►

Back | Close

Full Screen / Esc

Printer-friendly Version

Interactive Discussion
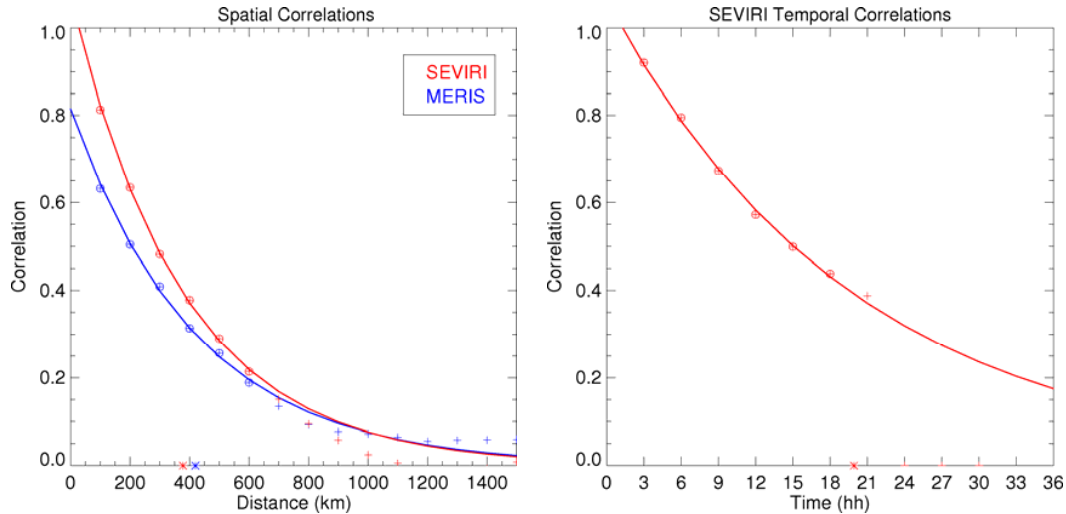
**Fig. 16.** Spatial (left) and temporal (right) correlation functions (crosses) for the total column water vapour as derived from bias corrected SEVIRI and MERIS data for August 2008. Points with an additional circle were used for the exponential fits (lines).
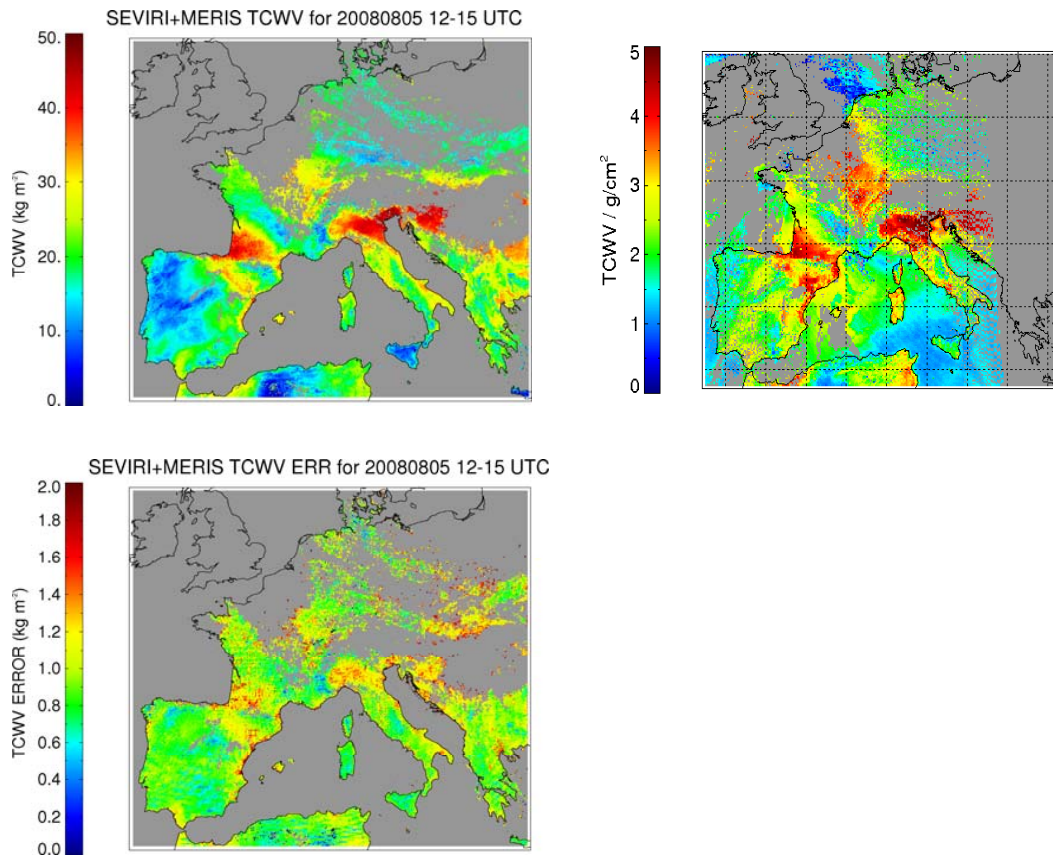
**Fig. 17.** Total column water vapour (top left) and error (bottom left) obtained from the Kriging of SEVIRI and MERIS for 5 August 2008 12:00–15:00 UTC. AQUA/MODIS total column water vapour (NASA LAADS MOYD05 product) for 5 August 2008 around 12:50 UTC (top right).